UNIVERSITY OF CALIFORNIA SAN DIEGO

Leak Detection in Fluid Distribution Networks

A dissertation submitted in partial satisfaction of the
requirements for the degree
Doctor of Philosophy

in

Engineering Sciences (Mechanical Engineering)

by

Abdulrahman Amin Alawadhi

Committee in charge:

Professor Daniel M. Tartakovsky, Chair
Professor Prabhakar Rao Bandaru, Co-Chair
Professor Marcos Intaglietta
Professor Ratneshwar Lal
Professor John Scott Mccartney

2019

The dissertation of Abdulrahman Amin Alawadhi is approved, and it is acceptable in quality and form for publication on microfilm and electronically:

_____

_____

_____

_____
Co-Chair

_____
Chair

University of California San Diego

2019

DEDICATION

To

My mother for keeping me in her prayers

My father for always encouraging me

My wife for never leaving me alone

My children for giving my life a new meaning

My siblings for being helpful and supportive

My mother and father in law for always being around my family

Everyone who helped me to be who I am

TABLE OF CONTENTS

LIST OF FIGURES

LIST OF TABLES

ACKNOWLEDGEMENTS

I would like to thank my advisor Professor Daniel M. Tartakovsky for being a great guidance during my last four years. He provided me with a continues support to produce this work. I would also like to thank my co-advisor Professor Prabhakar Rao Bandaru, and my committee members Professor Marcos Intaglietta, Professor Ratneshwar Lal, and Professor John Scott Mccartney.

Chapter 2, in full, is a reprint of the material as it appears in Method of distributions for water-hammer equations with uncertain parameters. Alawadhi, A.; Boso, F.; and Tartakovsky, D.M., Water Resource Research, 2018. The dissertation/thesis author was the primary investigator and author of this paper.

Chapter 3, in full, has been submitted for publication of the material as it may appear in Bayesian Updating and Method of Distributions: Application to Leak Detection in Pipes. Alawadhi, A.; and Tartakovsky, D.M., Water Resource Research, 2019. The dissertation/thesis author was the primary investigator and author of this paper.

Chapter 4, in full, has been submitted for publication of the material as it may appear in Leak Detection in Networks via Bayesian Update of the Method of Distributions. Alawadhi, A.; and Tartakovsky, D.M., Water Resource Research, 2019. The dissertation/thesis author was the primary investigator and author of this paper.

VITA

2004-2008	Undergraduate Student, Kuwait University
2008	Bachelor of Science in Mechanical Engineering, Kuwait University
2011-2012	Graduate Student, University of California San Diego
2012	Master of Science in Mechanical Engineering, University of California San Diego
2015-2019	Graduate Student Researcher, University of California San Diego
2019	Doctor of Philosophy in Engineering Sciences (Mechanical Engineering), University of California San Diego

ABSTRACT OF THE DISSERTATION

Leak Detection in Fluid Distribution Networks

by

Abdulrahman Amin Alawadhi

Doctor of Philosophy in Engineering Sciences (Mechanical Engineering)

University of California San Diego, 2019

Professor Daniel M. Tartakovsky, Chair
Professor Prabhakar Rao Bandaru, Co-Chair

Leakage is an undesired abnormality that causes economical losses and impacts the environment. Leak detection tests in pipe networks are usually interpreted using water-hammer equations (WHE). These equations are nonlinear hyperbolic partial differential equations (PDEs) used to describe transient flows in pipes. The associated uncertainties in initial and boundary conditions, parameters, and leak strength and location increases the stochastic behavior of these equations. The method of distributions is used to derive a deterministic PDE for probability density function (PDF) of pressure head and flow velocity under uncertain initial conditions. The derivation requires a closure approximation that ensures its consistency with the mean and the

variance of the state variables. A series of numerical experiments confirms the computational gain of this method over Monte Carlo simulations.

The PDF of pressure head obtained using the method of distributions serves as a prior PDF for data assimilation. Bayesian framework is used to update this distribution with a statistical model for observations obtained from the data collected by a pressure sensor. The result is posterior PDFs for leak location and leak strength. Series of numerical experiments are conducted for a single pipe and pipe networks under uncertain initial velocity and measurement noise to identify leak location and leak strength. The results are compared with the best fitness function that is used in inverse transient analysis.

1 Introduction

1.1 Introduction

Water is a vital natural resource. It is crucial for the environment and human beings. Water is usually transmitted through distribution networks from the source to the end user. These networks consist of a large number of interconnected pipes, and most of them are buried underground. This raises questions of the reliability of these pipes and leak detection.

As a pipe ages it becomes more susceptible to erosion and corrosion, which leads to unwanted abnormalities in the system. Brothers (2001) reported that real water losses in distribution and transmission systems are between 20% and 50%. An abnormality in any pipe can lead to high risk for human health. A partial blockage in a pipe due to contamination might be associated with a high concentration of harmful particles in drinking water. A leak is another abnormality that can introduce unhealthy materials to the distributed water. It also can impact the environment by discharging the fluid to the surrounding (Kirmeyer & Martel 2001, Karim et al. 2003). This risk might be even higher if the discharged fluid is a chemical other than water. These abnormalities are associated with potential economic losses as well. The wasted water through leakages decreases potential profits. This will also lead to increased use of energy to pay off for the wasted fluid. In addition to that, there will be a direct cost required for locating these abnormalities and repairing them. The World Bank estimated the global non-revenue water to be worth $14.7 billion per year (Thornton et al. 2008).

The common leak detection techniques are hardware based methods. Examples of these techniques are leak noise correlation (Muggleton & Brennan 2004, Gao et al. 2009), gas injection (Ratcliffe & Field 1978, Hargesheimer 1985), ground penetrating radar (O'Brien et al. 2003, Demirci et al. 2012), and acoustic sensing (Mergelas & Henrich 2005, Fletcher & Chandrasekaran 2008). Hardware based methods have high cost due to their need for equipment and manpower. Moreover, there might be significant delay between the time of leak occurrence and the time that these methods are used, especially for small leaks of which the facility owners are unaware.

Therefore, there is a need to have software based methods that are cheaper and can capture small leaks as soon as they occur. Since the pipes carry fluids, it is beneficial to utilize this fluid as a vehicle that delivers the information about any abnormalities.

Transient methods are the most promising software based methods since they require fewer sensors and can lead to a conclusion regarding the abnormality in shorter time than the steady state methods. Colombo et al. (2009) provide a comprehensive review on transient test based techniques (TTBTs). Direct transient approach (Jönsson & Larson 1992, Brunone 1999, Brunone & Ferrante 2001, Wang et al. 2002), frequency domain approach (Mpesha et al. 2001, Lee et al. 2005, Covas et al. 2005, Ghazali et al. 2012, Lee et al. 2013), and inverse transient analysis approach (Liggett & Chen 1994, Vítkovskỳ et al. 2000, 2007, Covas & Ramos 2010, Soares et al. 2011) are three approaches that fall under TTBTs.

1.2 Transient Test Based Techniques

The idea for TTBTs is based on a sudden change of pressure in a point, which creates a wave that travels to the sensor carrying information about the abnormality. In reservoir-pipe-valve system shown in figure 1.1, frictionless case will be used for demonstration, a pipe is connected between a reservoir and a valve. The system is assumed to have initial head pressure, H_{in}, and initial velocity u_0. A sudden closure of the end valve creates a wave traveling upstream. This wave increases the pressure head in the pipe to $H = H_{\text{in}} + \Delta H$ while reducing the velocity to zero $u = 0$ (Fig. 1.1a). As this wave reaches the reservoir, the pressure head reduces back to the initial pressure $H = H_{\text{in}}$ and this is associated with a velocity equal to the initial velocity but in the opposite direction, $u = -u_0$, with the wave traveling downstream (Fig. 1.1b). In figure 1.1c, the wave switches and starts to travel upstream after reaching the closed valve. This results in zero velocity $u = 0$ and a pressure head equal to $H = H_{\text{in}} - \Delta H$ behind the wave front. Finally (Fig. 1.1d), the wave returns back to travel downstream after it reaches the reservoir, but this

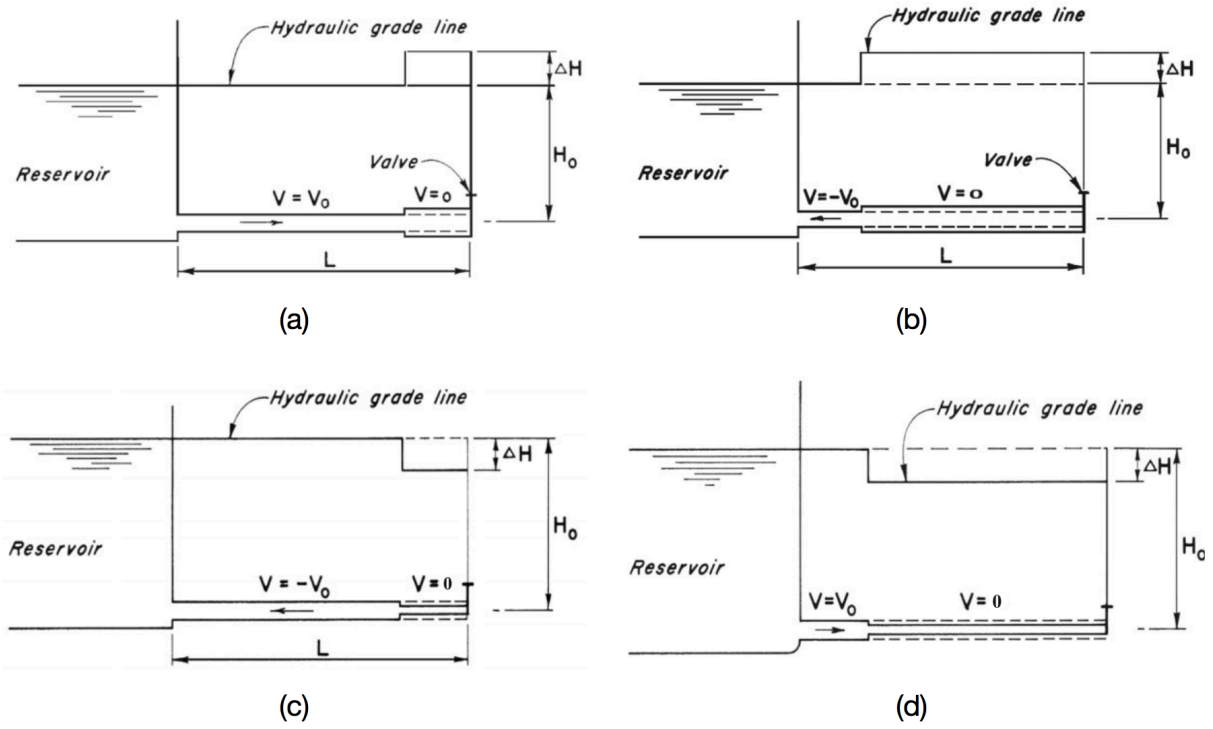

Figure 1.1: Propagation and reflection of a pressure wave in frictionless reservoir-pipe-valve system (Chaudhry 2013).

time the pressure head returns to $H = H_{\text{in}}$ with the velocity being equal to the initial velocity $u = u_0$ behind the wave front (the system returns back to the original conditions before shutting off the valve). This whole process can be described by one-dimensional water-hammer equations (Chaudhry 2013, Wylie et al. 1993), which is derived from the cross-sectionally averaged Navier-Stokes equations (Appendix A.1),

$$\frac{\partial h}{\partial t} + \frac{a^2}{g}\frac{\partial u}{\partial x} = 0 \tag{1.1a}$$

$$\frac{\partial u}{\partial t} + g\frac{\partial h}{\partial x} = k|u|u, \qquad k = -\frac{f}{2D} \tag{1.1b}$$

where $h(x,t)$ and $u(x,t)$ are cross-sectionally averaged pressure head and velocity, respectively, a is the wave speed, g is the gravitational acceleration, f is the Darcy-Weisbach friction factor. These equations can be solved with method of characteristics to obtain (Appendix A.2),

$$\frac{\mathrm{d}u}{\mathrm{d}t} + \frac{g}{a}\frac{\mathrm{d}h}{\mathrm{d}t} = k|u|u, \qquad \text{along} \qquad \frac{\mathrm{d}x}{\mathrm{d}t} = +a \tag{1.2}$$

$$\frac{\mathrm{d}u}{\mathrm{d}t} - \frac{g}{a}\frac{\mathrm{d}h}{\mathrm{d}t} = k|u|u, \qquad \text{along} \qquad \frac{\mathrm{d}x}{\mathrm{d}t} = -a. \tag{1.3}$$

Most of the software based methods rely on solving these equations and comparing the predicted response to the one obtained from the sensors to locate abnormalities. The methods succeeded in finding abnormalities in a single pipe. However, it is hard to obtain accurate results when it comes to networks, where many uncertainty and complexity are introduced. This is the reason of introducing a new method in this thesis to account for parametric uncertainty and measurement noise to obtain better results.

2 Method of Distributions for Water Hammer Equations With Uncertain Parameters

2.1 Introduction

Pipe networks are the main way for transporting fluids (e.g., water and hydrocarbons) from a reservoir to their final destination. However, as pipes age, they become prone to leakage due to corrosion. This raises environmental concerns and impacts public health when contaminants enter a compromised water distribution system or hydrocarbons spill into the ambient environment. Leaks also lead to economical losses due to wasted resources and repair costs. The World Bank estimates the global "nonrevenue" water, due to real and apparent losses and unbilled authorized consumption, to be worth $14.7 billion per year (Thornton et al. 2008); real water losses in distribution and transmission systems operated by water utilities are between 20% and 50% (Brothers 2001). Localizing and quantifying such losses is critical for monitoring the reliability of pipe networks and planning repairs.

Since leakage affects pressure and flow rate in a pipe, comparison between measurements of these quantities in a compromised pipe with their counterparts in the intact pipe could, in principle, be used to identify the location and intensity of a leak. However, each pipe in a network rarely contains more than one pressure gauge, so that pressure values at any location along a pipe (with and without a leak) must be inferred from an appropriate model. Practical and financial constraints on the number and positioning of measurement devices within a pipe network often result in the data being collected only upstream of a maneuver valve. Even if pressure measurements were available along the length of a pipe, the leak localization from steady-state pressure measurements would not be accurate. Consequently, transient test-based techniques were developed, mostly for single pipes (transmission mains) but also for laboratory pipe systems used to mimic distribution networks (Meniconi et al. 2015).

A popular leak-detection test involves an abrupt valve closure; it creates a contact-discontinuity wave moving upstream of the valve, which conveys information about fluid pressure and velocity to a sensor. This hydraulic regime is described by the cross-sectionally averaged

Navier-Stokes equations, which are called the water hammer equations (WHE) (Chaudhry 2013, Wylie et al. 1993). This experimental setup for leak detection and its interpretations with the WHE are reviewed in considerable detail by Colombo et al. (2009). (An alternative strategy, in which pressure waves along the pipes are generated by means of water injection (Brunone et al. 2008, Taghvaei et al. 2010), is not considered in this study). Relevant techniques for identification of a leak's location and intensity can be subdivided into forward methods (Brunone & Ferrante 2001, Wang et al. 2002) and inverse methods in the time (Vítkovskỳ et al. 2007, Massari, Yeh, Ferrante, Brunone & Meniconi 2013) and frequency (Mpesha et al. 2001, Covas et al. 2005) domains. In the first class of the inverse methods, several pressure transducers installed in the pipe system provide measurements, which are used to calibrate possibly very complex models of pressure and flow throughout the distribution system. In the second class, time or frequency pressure signals measured at a single location are analyzed as the system responds to a perturbation by comparing these readings to the no-leak conditions.

Predictability of WHE-based models and their use in conjunction with data are undermined by both uncertainty in the model parameters and measurement errors. Within the probabilistic framework both uncertain parameters and noisy data are treated as random quantities, and probabilistic model predictions are reported in terms of probability density functions (PDFs) of pressure and velocity or, more often, their ensemble means and (co)variances. These PDFs provide a complete probabilistic description of fluid flow in a pipe, including assessment of probabilities of rate events, and serve to quantify predictive uncertainty of WHE-based models. Probabilistic solutions of the WHE are also needed for identification of leaks and blockages in pipes by means of stochastic successive linear estimator (Massari et al. 2014) or data assimilation techniques based on Kalman filter (Ye & Fenner 2010).

Probabilistic solutions of the WHE can be obtained with Monte Carlo simulations (MCS) (Zhang et al. 2011, Duan 2015). This method is robust and easy to implement, but suffers from slow convergence and correspondingly high computational cost. If input parameters have

large correlation lengths, polynomial chaos expansions (Sattar & El-Beltagy 2016) are often, but not always (Barajas-Solano & Tartakovsky 2016), more efficient than MCS. The first-order perturbation analysis (Neuman et al. 1996) provides yet another alternative to MCS, which is appropriate for small variances of the input parameters and yields the means and variances of system states; it has been used in the WHE context by Massari, Yeh, Ferrante, Brunone & Meniconi (2013), Massari et al. (2014). Our goal is to derive and solve deterministic equations for the (joint) PDFs of pressure head and flow velocity governed by the stochastic WHE, without linearizing the latter and accounting for shocks.

The stochastic WHE are formulated in Section 2.2; they describe spatiotemporal evolution of cross-sectionally averaged fluid pressure head, $h(x,t)$, and velocity, $u(x,t)$, in a pipe following an abrupt closure of a valve. In Section 2.3, we derive a deterministic equation for the joint PDF of these two state variables, f_{hu}, which provides a full probabilistic description of the system's behavior at any point x along the pipe at any time t. In Section 2.4, we report a series of numerical experiments that demonstrate the accuracy and computational efficiency of this PDF equation by comparing its solution with the corresponding PDF estimated with Monte Carlo simulations. Major conclusions drawn from this study are summarized in Section 2.5.

2.2 Problem Formulation

We consider a pipe of length L and diameter D, which is equipped with a pressure sensor at $x = x^\star$ and a shut-off valve at the outlet $x = L$ (Fig. 2.1); it forms a part of a distribution network. Steady-state fluid flow in the pipe is pressure driven, with the inlet pressure head H_{in} exceeding the outlet pressure head H_{out} ($H_{\text{in}} > H_{\text{out}}$). A water hammer test are often conducted in an attempt to identify the location ($x = x_{\text{leak}}$) and intensity (Q_{leak}) of a leak. The leak intensity is defined as $Q_{\text{leak}}(h) = C_{\text{leak}} A_{\text{leak}} \sqrt{2gh} = \gamma_{\text{leak}} \sqrt{h}$, where C_{leak} and A_{leak} are the coefficient and area of discharge, respectively, and $\gamma_{\text{leak}} = C_{\text{leak}} A_{\text{leak}} \sqrt{2g}$. The test consists of an instantaneous, at time

$t = 0$, shutoff of the flow at the outlet, $u(x = L, t > 0) = 0$, and observing the pressure transients at the sensor.

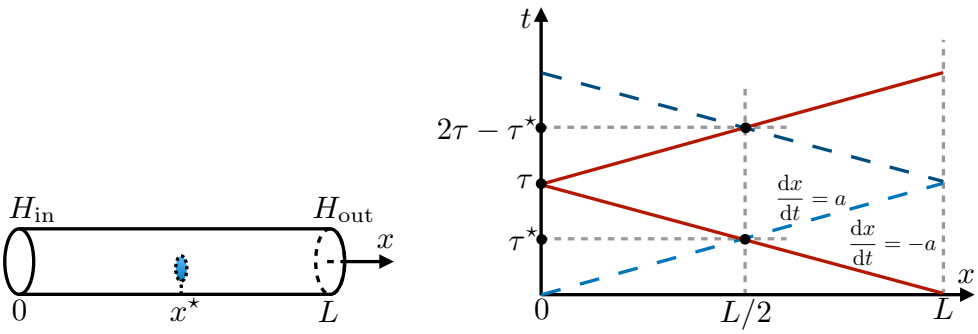

Figure 2.1: *Left*: A pipe of length L equipped with a pressure sensor and a valve located at $x = x^\star$ and $x = L$, respectively. At steady state, i.e., with the open valve, flow is driven by the difference in hydraulic heads at the inlet, H_{in}, and the outlet, H_{out}. *Right*: The contact discontinuities (waves), induced by the instantaneous (at time $t = 0$) closure of the valve, propagate with the wave speed a along two families of characteristics defined by $\mathrm{d}x/\mathrm{d}t = a$ and $\mathrm{d}x/\mathrm{d}t = -a$. The first contact discontinuity, traveling backward from the shut valve, reaches the sensor's location $x^\star = L/2$ at time $\tau^\star = L/(2a)$, and the pipe's inlet ($x = 0$) at time $\tau = L/a$. At that time, it turns into the second contact discontinuity that travels forward, reaching the sensor's location at time $2\tau - \tau^\star$.

Cross-sectionally averaged pressure head, $h(x,t)$, and velocity, $u(x,t)$, of the resulting turbulent flow in the pipe ($0 < x < L$) are governed by the (hyperbolic partial differential) WHE (Chaudhry 2013, Wylie et al. 1993),

$$\frac{\partial h}{\partial t} + \frac{a^2}{g}\frac{\partial u}{\partial x} = \frac{Q_{\text{leak}}}{A}\delta(x - x_{\text{leak}}) \tag{2.1a}$$

$$\frac{\partial u}{\partial t} + g\frac{\partial h}{\partial x} = k|u|u, \qquad k = -\frac{f}{2D} \tag{2.1b}$$

where a is the wave speed, g is the gravitational acceleration, f is Darcy-Weisbach friction factor. These equations describe the dynamics of contact discontinuities moving back and forth between the inlet and outlet (Fig. 2.1). The simplified model (2.1) relies on a quasi-steady state approximation of the wall shear stress (equating it to the squared local velocity), but the methodology presented below can also handle unsteady friction formulations.

These equations are subject to boundary conditions

$$h(x=0,t)=H_{\text{in}} \qquad \text{and} \qquad u(x=L,t)=0. \tag{2.2a}$$

The initial conditions for both u and h correspond to the steady-state condition of the system. It has a spatially uniform velocity u_0 and a spatially varying pressure head h_0, which is related to u_0 by the steady-state WHE,

$$h_0(x;u_0)=\frac{k}{g}|u_0|u_0x+H_{\text{in}}. \tag{2.2b}$$

The initial value u_0 is uncertain and treated as a random variable with prescribed PDF $f_{u_0}(U_0)$; the latter quantifies upon integration, e.g., the probability of u_0 not exceeding any given value U_0.

Consequently, predictions of $u(x,t)$ and $h(x,t)$ based on (2.1)–(2.2) are uncertain as well; their probabilistic description at a space-time point (x,t) is given by the joint PDF $f_{uh}(U,H;x,t)$. It can be used to compute, e.g., the probability of both flow velocity u exceeding a certain value U and pressure head h exceeding a certain value H. Estimating $f_{uh}(U,H;x,t)$ with MCS is computationally expensive and often prohibitively so if one has to reassemble an exhaustive set of MC runs for each potential leak location x_{leak}.

2.3 PDF Solutions to Water Hammer Equations

The main result of this study is the derivation in Appendix B.1 of a deterministic equation for the PDF $f_{uh}(U,H;x,t)$,

$$\frac{\partial f_{uh}}{\partial t}+\tilde{\nabla}\cdot(\mathbf{V}f_{uh})=0, \tag{2.3a}$$

where $\tilde{\nabla} = (\partial/\partial H, \partial/\partial U)^\top$ is the del operator in the phase space (H,U) of f_{uh}, and $\mathbf{V} = (V_H, V_U)^\top$ is the phase-space velocity with components

$$V_H = -\frac{a^2}{g}\frac{\partial \bar{u}}{\partial x} + \frac{Q_{\text{leak}}(H)}{A}\delta(x - x_{\text{leak}}) + \alpha_1(H - \bar{h}), \qquad V_U = -g\frac{\partial \bar{h}}{\partial x} + \alpha_2(U - \bar{u}) + k|U|U. \tag{2.3b}$$

Here, $\bar{u}(x,t)$ and $\bar{h}(x,t)$ are the ensemble means (averages) of random $u(x,t)$ and $h(x,t)$, respectively; $\sigma_u^2(x,t)$ and $\sigma_h^2(x,t)$ are their respective variances; and the coefficients α_1 and α_2 are given by (Appendix B.1)

$$\alpha_1 = -\frac{\gamma_{\text{leak}}\delta(x - x_{\text{leak}})}{2A\sqrt{\bar{h}}} + \frac{1}{2}\frac{\partial \ln \sigma_h^2}{\partial t} \qquad \text{and} \qquad \alpha_2 = -2k|\bar{u}| + \frac{1}{2}\frac{\partial \ln \sigma_u^2}{\partial t}. \tag{2.3c}$$

As demonstrated below, these statistics are computed with MCS at the fraction of the computational cost required to generate an MC sample sufficient for accurate estimation of the full PDF.

Probabilistic predictions of the pressure head $h(x,t)$ and flow velocity $u(x,t)$ separately are encapsulated in the marginal PDFs $f_u(U;x,t)$ and $f_h(H;x,t)$. These are defined from the joint PDF f_{uh} as $f_u(U;x,t) = \int f_{uh} \mathrm{d}H$ and $f_h(H;x,t) = \int f_{uh} \mathrm{d}U$. They satisfy the PDF equations,

$$\frac{\partial f_h}{\partial t} + \frac{\partial V_H f_h}{\partial H} = 0 \tag{2.4}$$

and

$$\frac{\partial f_u}{\partial t} + \frac{\partial V_U f_u}{\partial U} = 0, \tag{2.5}$$

which are derived by integrating (2.3) over U and H, respectively.

The joint/marginal PDF equations (2.3)–(2.5) are subject to initial and boundary condi-

tions, that reflect the information about the initial and boundary conditions of the physical system. Specifically, the initial condition for (2.3) is given in terms of the joint PDF of the initial states u_0 and h_0, $f_{u_0h_0}(U,H;x)$. Given f_{u_0}, the (marginal) PDF of u_0, the latter is expressed in terms of the conditional PDF $f_{h_0|u_0}$ as $f_{u_0h_0} = f_{h_0|u_0}f_{u_0}$. Since (2.2b) provides a deterministic relation between u_0 and h_0, knowledge of the former completely determines the latter, i.e., $f_{h_0|u_0} = \delta(H - h_0)$.

Since the PDF equations (2.3)–(2.5) do not contain spatial derivatives, the space coordinate x acts as a parameter. Consequently, one can obtain the PDFs of u and h only at points where they are needed for data assimilation, e.g., where the pressure sensors are deployed.

2.4 Simulation Results

In the simulations reported below, we consider fluid flow in a pipe of length $L = 3000$ m and diameter $D = 0.5$ m, and with the Darcy-Weisbach friction factor $f = 0.03$. An instantaneous closure of the valve at the outlet ($x = L$) creates a transient wave whose speed is $a = 1403$ m/s; the constant pressure head $H_{\text{in}} = 150$ m is maintained at the pipe's inlet ($x = 0$). The pipe is assumed to be intact, i.e., $Q_{\text{leak}} = 0$. The time required for the contact discontinuity to travel from the valve back to the inlet is $\tau = L/a = 2.14$ s, and the time required for the contact discontinuity to reach the point of interest (sensor) $x^\star = L/2 = 1500$ m is $\tau^\star = (L - x^\star)/a = 1.07$ s. The simulation time horizon is set to $T = 5$ s, which covers the first two contact discontinuities passing through the sensor. The uncertain initial velocity u_0 is modeled as a lognormal random variable such that $u_0 = 2.0 + 0.1\exp(z)$, where z is a Gaussian random variable with mean $\mu_z = 0$ and standard deviation $\sigma_z = 0.4$. This translates into the mean $\mu_{u_0} = 2.1$ m/s and standard deviation $\sigma_{u_0} = 0.045$ m/s of the lognormal initial velocity u_0, such that 96% of the values of u_0 fall between 2.0 m/s and 2.2 m/s.

We use a set of 30000 Monte Carlo realizations as a yardstick against which the accuracy and computational efficiency of the method of distributions are ascertained. For each realization

of u_0, the interval $(0, L)$ is discretized into 60 elements and the WHE (2.1) are solved using the method of characteristics with the explicit finite-difference method Chaudhry (2013), Wylie et al. (1993). Monte Carlo estimates of the PDFs of $h(x,t)$ and $u(x,t)$ are obtained using a Gaussian kernel density estimator (KDE) provided by the Matlab function `ksdensity`, which automatically estimates the KDE bandwidth. The sampling errors in computing the mean ($\mathcal{E}_{\bar{h}}$) and variance ($\mathcal{E}_{\sigma_h^2}$) of $h(x^\star, t = 3.14 \text{ s})$ from N_{MC} Monte Carlo realizations ($N_{\text{MC}} \leq 30000$), as well as the corresponding errors $\mathcal{E}_{\alpha_1}$ and $\mathcal{E}_{\alpha_2}$ in estimating the mixed ensemble moments α_1 and α_2, are defined as

$$\mathcal{E}_{\mathcal{A}}(N_{\text{MC}}) = \left| \frac{\mathcal{A}(30000) - \mathcal{A}(N_{\text{MC}})}{\mathcal{A}(30000)} \right|, \qquad \mathcal{A} = \bar{h}, \sigma_h^2, \alpha_1, \alpha_2. \tag{2.6}$$

A sampling error in estimation of $f_h(H; x^\star, t = 3.14 \text{ s})$, the PDF of $h(x^\star, t = 3.14 \text{ s})$, is reported in terms of the Kullback-Leibler (KL) divergence between $f_h(H; x^\star, t = 3.14 \text{ s})$ estimated from 30000 Monte Carlo realizations of $h(x^\star, t = 3.14 \text{ s})$, $f_{h,30000}$, which is treated as ground truth, and its counterpart computed with a smaller number of realization N_{MC}, $f_{h,N_{\text{MC}}}$. The latter is defined as

$$\mathcal{E}_{f_h}(N_{\text{MC}}) \equiv D_{\text{KL}}(f_{h,N_{\text{MC}}}, f_{h,30000}) \equiv \int f_{h,N_{\text{MC}}} \ln \left(\frac{f_{h,N_{\text{MC}}}}{f_{h,30000}} \right) \mathrm{d}H. \tag{2.7}$$

As expected, all five sampling errors in (2.6) and (2.7) decrease as the number of Monte Carlo realizations N_{MC} increases (Fig. 2.2). The sampling errors in estimating the means, $\bar{h}$ and $\bar{u}$, and the closure variable α_1 fall below 10^{-3} after $N_{\text{MC}} \approx 1000$ realizations, while no less than $N_{\text{MC}} = 30000$ realizations are required to estimate the PDFs of h and u with the same accuracy. While the sampling error $\mathcal{E}_{\alpha_2}(N_{\text{MC}} = 1000) = O(10^{-2})$, its effect on the overall predictive error is diminished by the fact that α_2 in (2.3)–(2.5) is multiplied by $(U - \bar{u})$ which, during the time period of significance for leak detection tests (see below), is $O(10^{-2})$. Since only $\bar{u}$, $\bar{h}$, α_1 and α_2 are used in the PDF equations (2.3)–(2.5), the use of the latter to obtain PDFs results in significant computation saving.

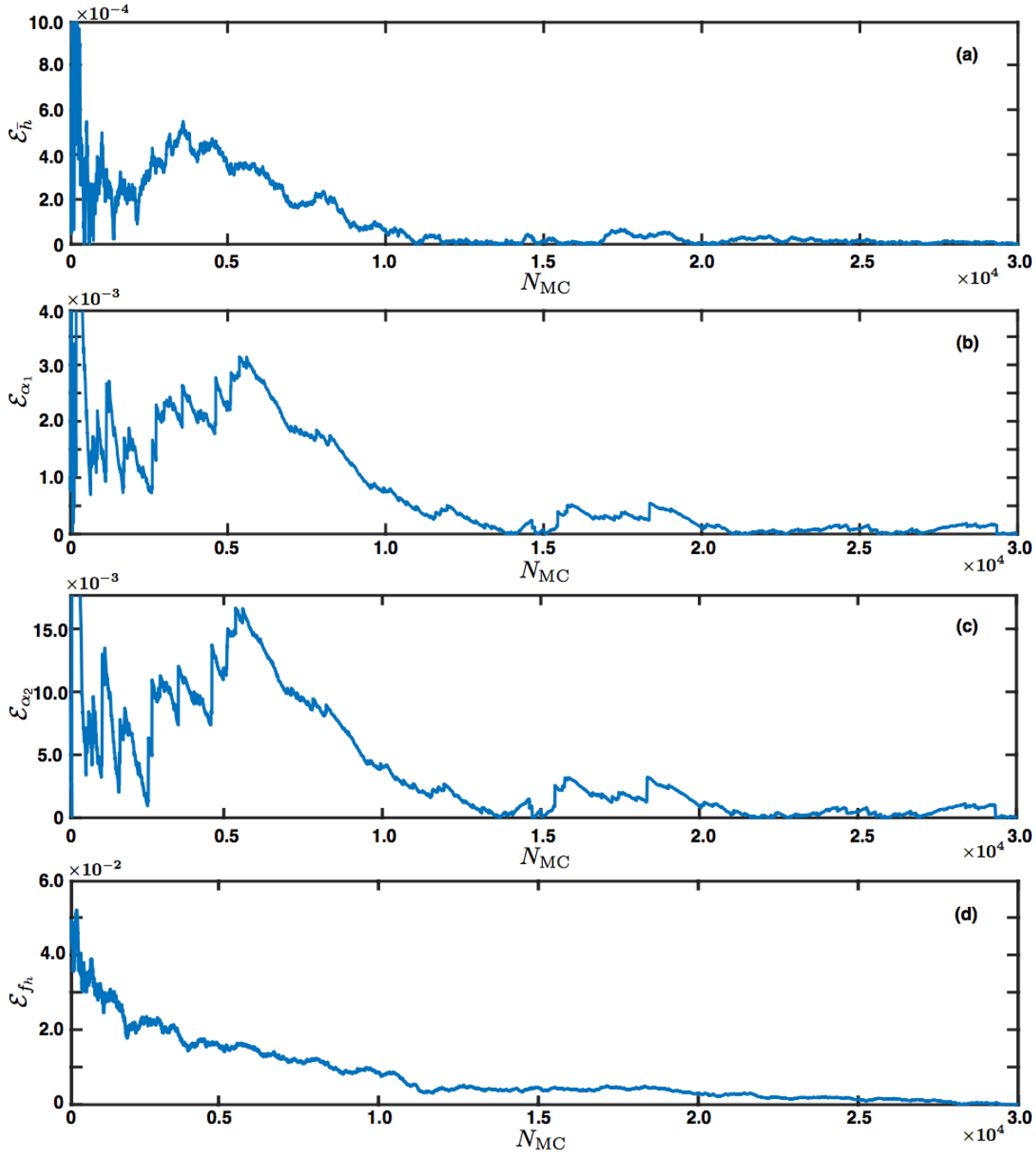

Figure 2.2: Sampling errors in estimating, from N_{MC} Monte Carlo realizations, the sample mean (a) and PDF (d) of the pressure head h in the middle of the pipe ($x = 1500$ m) after the first contact discontinuity passed through it (at time $t = 3.14$ s). Also shown are the corresponding sampling errors in estimating the closure variables α_1 (b) and α_2 (c). All the errors are defined in (2.6) and (2.7).

The coefficients in PDF equations (2.3)–(2.5) exhibit jump discontinuities at space-time points wherein the forward and backward waves traveling along the corresponding two families of characteristics intersect (see Appendix B.3 for detail). These discontinuities can be handled either with an appropriate numerical method or, as we do in Appendix B.3 for the leak-free flows, analytically by taking advantage of the fact that their dynamics are deterministic.

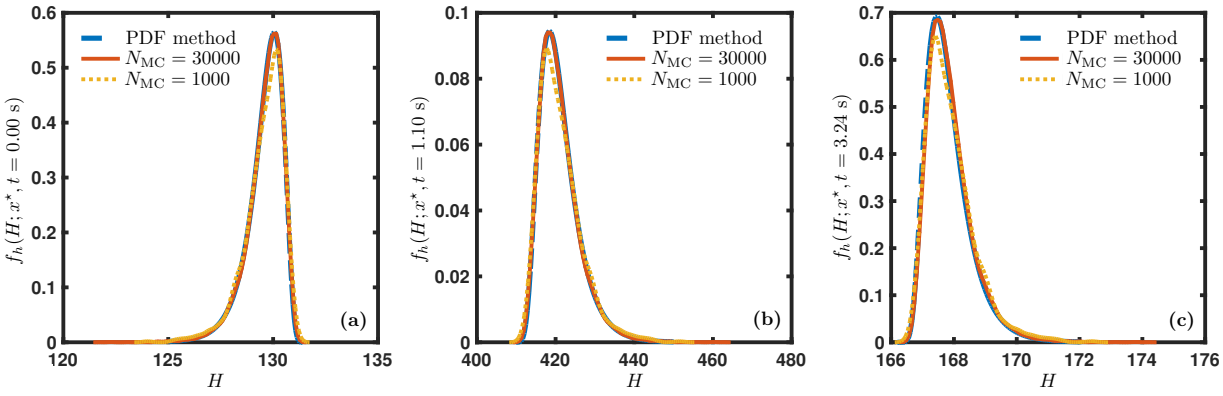

Figure 2.3: Temporal snapshots of the PDF $f_h(H;x^\star,t)$ of the pressure head $h(x,t)$ at the observation point $x = x^\star$ obtained analytically in Appendix B.3 (dashed line) or by using the kernel density estimator to post-process $N_{\mathrm{MC}} = 30000$ (solid line) and $N_{\mathrm{MC}} = 1000$ (dotted line) Monte Carlo realizations. The results are presented at $x^\star = L/2$ (the middle of the pipe), for three times t: at initial time $t = 0.00$ s (a); and the times $t = 1.10$ s (b) and $t = 3.24$ s (c) at which the first and second contact discontinuities pass over $x^\star$, respectively.

Figure 2.3 exhibits the marginal PDF $f_h(H,x^\star,t)$ for the pressure head $h(x,t)$ in the sensor location, $x^\star = L/2$, before the first contact discontinuity (a), after the first contact discontinuity (b), and after the second contact discontinuity (c) pass through it. These PDFs are alternatively computed with the PDF method and Monte Carlo simulations comprising $N_{\mathrm{MC}} = 1000$ and $N_{\mathrm{MC}} = 30000$ realizations. The solution of the PDF equation, whose parametrization relies on $N_{\mathrm{MC}} = 1000$ realizations, agrees with the PDF estimate based on $N_{\mathrm{MC}} = 30000$ realizations: the difference between these two solutions, as quantified by the KL divergence, is $\mathcal{E}_{f_h} = 0.0017$. The MCS estimate of f_h achieves the same accuracy with $N_{\mathrm{MC}} \approx 6000$ realizations, which takes about three times longer to compute than the PDF method does. If one were to rely on the Kolmogorov-Smirnov test, $\mathcal{E}^{\mathrm{KS}}_{f_h} = \sup_H |f_{h,N_{\mathrm{MC}}} - f_{h,30000}|$, as a measure of the difference

between the "exact" and approximate PDFs then the PDF method is nine times faster than MCS (one needs $N_{\mathrm{MC}} \approx 19000$ realizations to achieve the error $\mathcal{E}_{f_h}^{\mathrm{KS}} = 0.0016$ of the PDF method), with an even larger computational gain. The comparison between the PDF estimates provided by the PDF method and Monte Carlo simulations with $N_{\mathrm{MC}} = 30000$ realizations in Figures 2.3 and 2.4 validates the accuracy of the closure approximation, which underpins the derivation of our deterministic PDF equation (2.4).

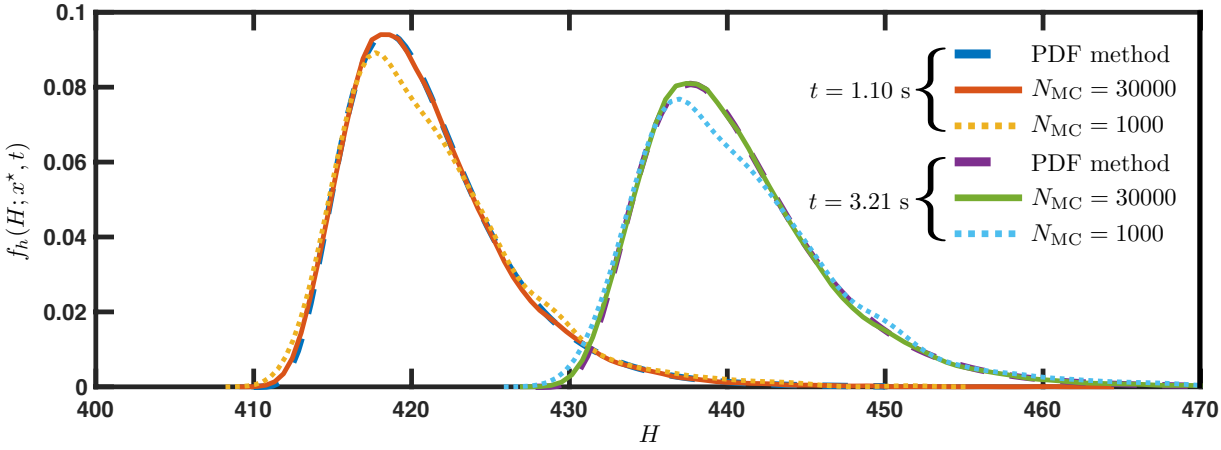

Figure 2.4: Temporal snapshots of the PDF $f_h(H;x^\star,t)$ of the pressure head $h(x,t)$ at the observation point $x = x^\star$ obtained, alternatively, by solving the PDF equation (2.4) (dashed line) or by using the kernel density estimator to post-process $N_{\mathrm{MC}} = 30000$ (solid line) and $N_{\mathrm{MC}} = 1000$ (dotted line) Monte Carlo realizations. The results are presented at $x^\star = L/2$ (the middle of the pipe) for the time interval during which the first contact discontinuity passed through $x^\star$ ($t = 1.10$ s) and just before the second contact discontinuity has reached it ($t = 3.21$ s).

The support of the PDF $f_h(H;\cdot)$, i.e., a set of values of H for which $f_h(H;\cdot) \neq 0$, changes with time; the predictive uncertainty (pressure variance σ_h^2 or the PDF width) is significantly larger after the passage of the first contact discontinuity (Fig. 2.3b) than the second one (Fig. 2.3c). That is why many leak-detection techniques focus on the time interval after the first contact discontinuity to determine the leak location and size, taking advantage of the fact that during this time the pressure is highest and the effects of a leak are magnified (Covas et al. 2008). Damping in the periodic wave gives the first cycle the advantage over the other cycles since the leak effect is at its peak. In general, the pressure PDF f_h and its moments (e.g., the mean

and variance of h) are discontinuous at the moving wave front. In between the two adjacent waves carrying, e.g., the first and second contact discontinuities, the pressure $h(x,t)$ is continuous and the impact of uncertain parameters increases with time (Fig. 2.4); therefore, pressure (and velocity) measurements collected during that time interval have higher information content (i.e., their assimilation would have a higher impact on reduction of the predictive uncertainty) than the data collected at other times.

The fluid pressure PDF $f_h(H;\cdot)$ remains highly asymmetric (non-Gaussian) at all times, with skewness that changes sign during the time cycle considered (Fig. 2.3). This suggests that data assimilation strategies based on different flavors of the Kalman filter are suboptimal and might yield erroneous estimators of the system states and inputs (e.g., the location and intensity of a leak). Instead, one might have to deploy Bayesian strategies, which would treat the PDF $f_h(H;\cdot)$ computed with our PDF equations as a prior distribution and then use pressure measurements to construct a posterior PDF.

The PDFs in Figures 2.3 and 2.4 quantify the uncertainty in predictions of the fluid pressure dynamics stemming from uncertain initial conditions in an intact pipe. In the presence of a leak, the pressure signals typically display faster damping and more complex wave reflections. Figure 2.5 demonstrates this effect by comparing the pressure PDFs in leaky and intact pipes; in both cases the initial velocity is set to $u_0 = 2.1$ m/s and, for the leaky pipe, the leak parameter is set to $C_{\text{leak}}A_{\text{leak}} = 0.0001$ m^2. The PDF behavior is significantly affected by the presence of the leak, the most apparent feature being a significant shift of the PDF towards lower pressure values.

The comparison of PDFs in leak and no-leak conditions might help one to identify locations where the difference between the two scenarios is the largest as the the most affected by potential leaks and the most advantageous for measurement collection when sensor placing is yet to be determined. In all other cases, it represents a physically-based prior distribution to be updated via data assimilation for uncertainty reduction and possibly leak detection.

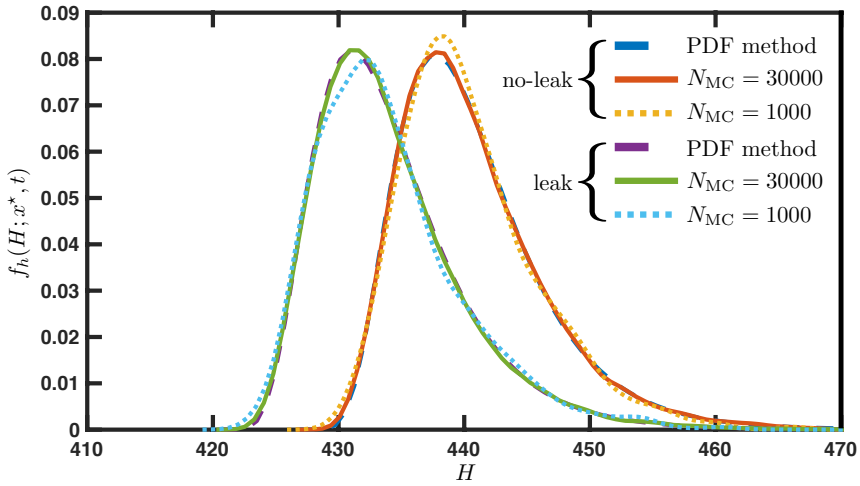

Figure 2.5: Temporal snapshots of the PDF $f_h(H;x,t)$ of the pressure head $h(x,t)$ for an intact pipe and a pipe with leak at point $x_{\text{leak}} = 2450$ m with uncertain initial conditions. The results are presented at the middle of the pipe, $x = x^\star$, at time $t = 3.21$ s.

2.5 Conclusions

We developed a deterministic partial-differential equation for the joint probability density function (PDF) of the fluid pressure and flow velocity in a pipe. The latter are governed by the water hammer equations for hydraulic transients following the valve shut-down. Our probabilistic approach accounts for uncertainty in initial and boundary conditions for the system, and represents a computationally efficient alternative to Monte Carlo simulations.

The closure of the PDF equation relies on the knowledge of the time evolution of the first- and second-order moments (i.e., the mean and variance of pressure and velocity) in a specific location along the pipe. We demonstrate how using a subset of Monte Carlo simulations (MCS) to compute the moments (and consequently the closures) for the PDF equation yields the same accuracy in the PDF as obtained via MCS using the full set of realizations, resulting in significant computational savings.

The (joint) PDF obtained as a solution of the PDF equation represents a physically-based prior distribution for pressure and/or velocity, which lends itself to assimilation of flowmeters and pressure transducers measurements. Data can thus be used for parameter identification and

for leakage/blockage detection.

2.6 Acknowledgments

Chapter 2, in full, is a reprint of the material as it appears in Method of distributions for water-hammer equations with uncertain parameters. Alawadhi, A.; Boso, F.; and Tartakovsky, D.M., Water Resource Research, 2018. The dissertation/thesis author was the primary investigator and author of this paper.

3 Bayesian Updating and Method of Distributions: Application to Leak Detection in Pipes

3.1 Introduction

Underground water distribution networks are susceptible to leakage, especially as pipes age due to mechanical fatigue and corrosion. Compromised pipes raise environmental concerns and might impact public health if contaminants enter a distribution system. Perhaps more significant, leaks lead to economical losses due to the wasted resources and the cost and time required for repair. Water losses in distribution and transmission systems are estimated to be between 20% and 50% for water utilities (Brothers 2001). This dire situation, caused by the perennial lack of funds needed to upgrade water distribution systems, puts a special premium on monitoring the reliability of pipe networks in order to localize leaks and to decrease time and cost of repairs.

Leakage is a hydraulic process that affects the pressure and flow rate in pipes. This makes tracking hydraulic characteristics and comparing them to their counterparts for intact pipes a natural way to identify leak location and size. Unfortunately, the scarcity of pressure gauges and their accuracy in pipe networks complicate this procedure at steady state. Consequently, contemporary leak detection typically relies on transient test-based techniques (TTBTs), in which a valve downstream of the valve or water injection devices is abruptly closed to induce unsteady flow (Taghvaei et al. 2010, Brunone et al. 2008); this procedure also creates a pressure discontinuity, which travels upstream of the pipe and carries the information about a leak to the sensors. This procedure is modeled by water-hammer equations (WHE) (Wylie et al. 1993, Chaudhry 2013), hyperbolic partial differential equations obtained by cross-sectional averaging of Navier-Stokes equations. A comprehensive review of TTBTs is provided by Colombo et al. (2009). One of these techniques is the inverse transient analysis, which minimizes the difference between pressure measurements and (numerical) solutions of WHE to locate defects (Liggett & Chen 1994, Vítkovskỳ et al. 2000, 2007). This method requires multiple pressure sensors. Another technique is referred to as the direct transient approach. It looks for a defect in the pressure signal

passing through a sensor (Brunone 1999, Brunone & Ferrante 2001, Wang et al. 2002). The third techniques is called the frequency domain method; it involves a periodically actuated device with pressure measurements confined to a part of a network or of a single pipe (Mpesha et al. 2001, Lee et al. 2005, Covas et al. 2005).

These and other similar techniques assume the model parameters and operating conditions to be known with certainty (deterministic). This is seldom the case in water distribution networks that suffer from variable/uncertain demand levels, build ups on pipes, etc. The probabilistic framework, which equates uncertainty with randomness, provides a natural way of dealing with such complications. Some of the probabilistic approaches used to account for uncertainty in WHE are Monte Carlo simulations (MCS) (Zhang et al. 2011, Duan 2015), polynomial chaos expansions (Sattar & El-Beltagy 2016), and the method of distributions (Alawadhi et al. 2018). Instead of giving a single prediction of fluid pressure, these methods yield its probability density function (PDF), which can be used to assign the likelihood of occurrence (probability) to a particular prediction. It can also be used for Bayesian updating to assimilate the pressure data into model predictions, facilitating detection of leaks and estimation of their strength.

Among various data assimilation techniques, which include variational methods (Bannister 2017), stochastic successive linear estimator (Massari, Yeh, Brunone, Ferrante & Meniconi 2013, Massari et al. 2014), and different variants of Kalman filter (Ye & Fenner 2010), we select Bayesian updating (Wikle & Berliner 2007) because it can handle nonlinear non-Gaussian systems. Rougier & Goldstein (2001) used Bayesian analysis for pipelines with uncertain characteristics, and showed that this method refines the belief about the pressure and flow. Despite its strengths, Bayesian data assimilation is notoriously computationally expensive, in part because it requires a large number of MC realizations to estimate a system state's PDF. We accelerate this step by deploying the method of distributions, which provides the prior PDF of pressure at the fraction of the computational cost of MCS (Alawadhi et al. 2018).

Our paper is organized as follows. Section 3.2 contains a problem formulation and

introduces WHE with random inputs. Its solution, given in terms of the PDF of fluid pressure in a pipe, is presented in Section 3.3. This solution serves as a prior for Bayesian data assimilation, which is used in Section 3.4 to locate a leak. Results of our numerical experiments are reported in Section 3.5. Major conclusions drawn from this study are summarized in Section 3.6.

3.2 Problem Formulation

Following the standard practice, we consider a reservoir-pipe-valve system (Fig. 3.1), which represents a transmission main as a pipe of length L and diameter D. The pipe is equipped with a sensor located at $x = x^\star$ and a shutoff valve at the pipe outlet $x = L$. A water-hammer test consists of instantaneous shut off of the downstream valve at time $t = 0$, which creates a pressure wave traveling upstream, and monitoring the pressure response at the sensor. The signal carried towards the sensor is used to identify leak location (x_{leak}) and its intensity (Q_{leak}). Prior to the shut off, the flow is assumed to be steady.

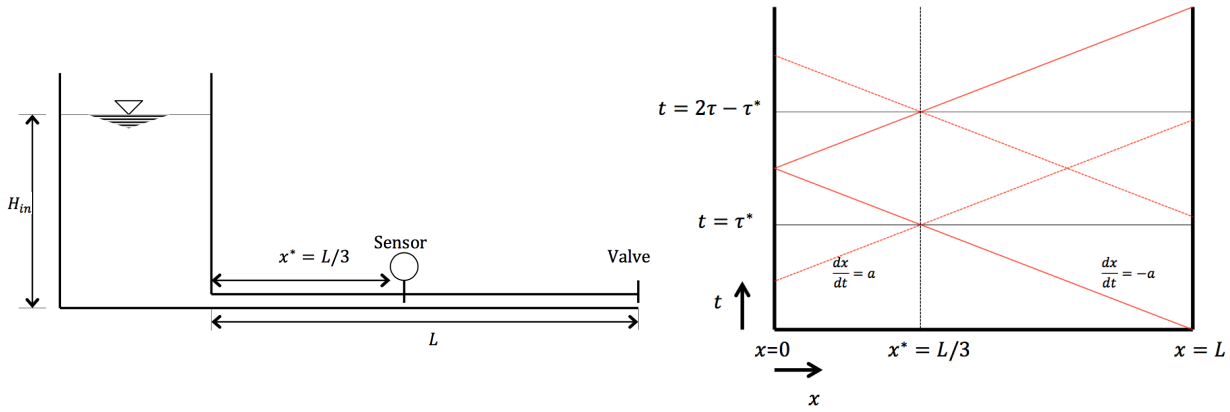

Figure 3.1: *Left*: A reservoir-pipeline-valve system. *Right*: Space-time domain with the time that the shock passes through a sensor located at $x^\star$.

This test is described by WHE (Chaudhry 2013, Wylie et al. 1993), which predict the

response of cross-sectionally averaged pressure head, $h(x,t)$, and velocity, $u(x,t)$:

$$\frac{\partial h}{\partial t} + \frac{a^2}{g}\frac{\partial u}{\partial x} = \frac{Q_{\text{leak}}}{A}\delta(x - x_{\text{leak}}) \tag{3.1a}$$

$$\frac{\partial u}{\partial t} + g\frac{\partial h}{\partial x} = k|u|u, \qquad k = -\frac{f}{2D} \tag{3.1b}$$

where a is the wave speed; g is the gravitational acceleration constant; $A = \pi D^2/4$ is the cross-sectional area of the pipe; f is Darcy-Weisbach friction factor; x_{leak} and Q_{leak} are the unknown location and strength of the leak, respectively; and $\delta(\cdot)$ is the Dirac delta function used to represent the leak as a point source/sink.

Boundary conditions for (3.1) are

$$h(x = 0,t) = H_{\text{in}} \qquad \text{and} \qquad u(x = L,t) = 0, \tag{3.2a}$$

where H_{in} is the prescribed pressure head at the pipe inlet. The initial conditions are obtained from the steady-state conditions before the valve shut off. The initial velocity u_0 is uniform along the pipe, while the corresponding initial pressure head h_0 is spatially varying and related to u_0 by the steady-state WHE,

$$h_0(x;u_0) = \frac{k}{g}|u_0|u_0 x + H_{\text{in}}. \tag{3.2b}$$

Since $\delta(x - x_{\text{leak}}) = 0$ for $x \neq x_{\text{leak}}$, Eqs. (3.1) can be replaced with their homogeneous counterparts defined on the sub-domains $0 < x < x_{\text{leak}}$ and $x_{\text{leak}} < x < L$. Solutions of these homogeneous equations on the two sub-domains are coupled by the interfacial conditions at $x = x_{\text{leak}}$. One of these conditions is pressure continuity, $h(x_{\text{leak}}^-,t) = h(x_{\text{leak}}^+,t)$, where the subscripts $^-$ and $^+$ indicate the limits of $h(x,t)$ as $x \to x_{\text{leak}}$ from the left and the right of x_{leak},

respectively. The second condition stems from mass conservation (Brunone 1999),

$$Q^- = Q^+ + Q_{\text{leak}}, \qquad Q_{\text{leak}}(t) = C_L A_L \sqrt{2gh(x = x_{\text{leak}}, t)}, \tag{3.2c}$$

and relates the flow rates upstream, $Q^- \equiv Q(x^-_{\text{leak}}, t)$, and downstream, $Q^+ \equiv Q(x^+_{\text{leak}}, t)$, of the leak. Here C_L and A_L are the discharge coefficient and the leak area, respectively.

In addition to x_{leak} and Q_{leak}, we allow the initial velocity u_0 to be uncertain. The latter uncertainty is quantified by treating u_0 as a random variable with prescribed PDF $f_{u_0}(U_0)$. In the absence of additional information, we assign to x_{leak} and $C_L A_L$ the uniform (uninformative) prior PDFs on the intervals $(0, L)$ and $[\mathcal{A}_{min}, \mathcal{A}_{max}]$, respectively:

$$x_{\text{leak}} = \mathcal{U}(0, L) \quad \text{and} \quad C_L A_L = \mathcal{U}[\mathcal{A}_{min}, \mathcal{A}_{max}]$$

We also account for measurement errors affecting the pressure sensor readings $h_{\text{obs}}(t)$,

$$h_{\text{obs}}(t) = h(x^\star, t) + \xi(t), \tag{3.3}$$

where $\xi(t)$ is the zero-mean Gaussian white noise with variance σ^2_ξ, i.e., $\mathbb{E}[\xi(t)] = 0$ and $\mathbb{E}[\xi(t_1)\xi(t_2)] = \sigma^2_\xi \delta(t_1 - t_2)$.

A goal of Bayesian updating is to refine the uninformed estimates of x_{leak} and $C_L A_L$ by combining the probabilistic predictions provided by (3.1) and (3.2) with observations (3.3). The PDF of $h(x,t)$, the solution of (3.1) and (3.2), is computed in Section 3.3. Our strategy for Bayesian updating of this prior PDF with data (3.3) is detailed in Section 3.4.

3.3 Method of distributions

When applied to (3.1) and (3.2), the method of distributions (Tartakovsky & Gremaud 2015) yields a deterministic equation for the PDF $f_h(H;x,t)$ of the pressure head $h(x,t)$ (Alawadhi et al. 2018),

$$\frac{\partial f_h}{\partial t}+\frac{\partial V f_h}{\partial H}=0, \qquad V=-\frac{a^2}{g}\frac{\partial \bar{u}}{\partial x}+\frac{Q_{\text{leak}}}{A}\delta(x-x_{\text{leak}})-\alpha_1(H-\bar{h}). \tag{3.4a}$$

This equation describes advection of a passive scalar, f_h, in the velocity field $V(h,H,t)$. The latter depends explicitly on the mean flow velocity $\bar{u}(x,t)$ and the mean pressure head $\bar{h}(x,t)$, and implicitly on the pressure head variance $\sigma_h^2(x,t)$, through the closure variable α_1 that is given by

$$\alpha_1=-\frac{C_L A_L\sqrt{2g}\delta(x-x_{\text{leak}})}{2A\sqrt{\bar{h}}}+\frac{1}{2}\frac{\partial \ln\sigma_h^2}{\partial t}. \tag{3.4b}$$

These low-order statistics can be computed via, e.g., moment-differential equations (MDEs) for (3.1) and (3.2). Instead, we compute them with Monte Carlo simulations (MCS) to avoid the closure approximations that underpin the derivation of MDEs. This strategy is computationally more efficient than MCS estimation of f_h, since it take significantly few MC realization to compute, with prescribed accuracy, the low moments than the full PDF.

The PDF equation (3.4) is subject to the initial and boundary conditions that reflect the degree of certainty in the initial and boundary conditions of the physical system. This is done by relating the output pressure head h_i to the initial velocity u_0 after ith discontinuity ($i=1,2,\cdots$). This relation is obtained as follows. From the PDF f_{u_0}, we draw N realizations of u_0, denoted by $u_0^{(1)},\cdots u_0^{(N)}$. For each of these realizations, the WHE (3.1) is solved numerically by means of the method of characteristic with explicit finite differences Chaudhry (2013) to obtain the values of the pressure heads after the ith discontinuity, $h_i=h_i(u_0)$, $i=1,2,\cdots$. This procedure results in an array of data $\{u_0^{(k)},h_i^{(k)}\}_{k=1}^N$. Then, we fit a second-order polynomial, $u_0=\alpha_i h_i^2+\beta_i h_i+\gamma_i$,

to these data, i.e., find the coefficients α_i, β_i, and γ_i that minimize the mean root square error between the polynomial and the data. Once the map between u_0 and h_i is available, the PDF of the pressure head after each discontinuity is obtained as

$$f_{h_i} = \left| \frac{\mathrm{d}u_0}{\mathrm{d}h_i} \right| f_{u_0} \qquad \text{where} \qquad u_0 = \alpha_i h_i^2 + \beta_i h_i + \gamma_i. \tag{3.5}$$

Equations (3.4) and (3.5) are solved multiple times, for each node x_{leak} on the discretized interval $(0, L)$, to obtain $f_{h|x_{\text{leak}}}(H; x, t)$, the conditional PDF for the pressure head $h(x,t)$ given the leak location at $x = x_{\text{leak}}$. Since the PDF equation (3.4a) does not contain spatial derivatives, the physical space coordinate x acts as a parameter in this equation. Hence, it is sufficient to solve (3.4) and (3.5) only for the sensor node $x = x^\star$. The resulting conditional PDF $f_{h|x_{\text{leak}}}(H; x^\star, t)$ is used for data assimilation.

3.4 Data Assimilation

Once the conditional PDF $f_{h|x_{\text{leak}}}(H; x^\star, t)$ is computed by solving the PDF equation, the joint PDF between h and x_{leak}, $f_{h,x_{\text{leak}}}(H, X; x^\star, t)$, is computed as

$$f_{h,x_{\text{leak}}}(H, X; x^\star, t) = f_{h|x_{\text{leak}}}(H; x^\star, t) f_{x_{\text{leak}}}(X) \tag{3.6}$$

where $f_{x_{\text{leak}}}(X)$ is the prior PDF of the leak location, e.g., uniform PDF on $[0, L]$ to reflect the lack of prior knowledge. Bayesian updating (Wikle & Berliner 2007) requires a statistical model for observations, $f_{h_{\text{obs}}|h,x_{\text{leak}}}$, which is obtained from sensor readings. Then, the posterior distribution $f_{h,x_{\text{leak}}|h_{\text{obs}}}(H, X; x^\star, t)$ is computed with the Bayes formula,

$$f_{h,x_{\text{leak}}|h_{\text{obs}}} = \frac{f_{h_{\text{obs}}|h,x_{\text{leak}}} f_{h,x_{\text{leak}}}}{f_{h_{\text{obs}}}}, \qquad f_{h_{\text{obs}}} = \int f_{h_{\text{obs}}|h,x_{\text{leak}}} f_{h,x_{\text{leak}}} \mathrm{d}H \tag{3.7}$$

where $f_{h_{\text{obs}}}$ is a normalizing constant. Finally, the posterior PDF $f_{x_{\text{leak}}}(X)$ is computed as the marginal of $f_{h,x_{\text{leak}}|h_{\text{obs}}}$, i.e., by computing the integral $f_{x_{\text{leak}}|h_{\text{obs}}} = \int f_{h,x_{\text{leak}}|h_{\text{obs}}} \mathrm{d}H$. This new PDF can then be used as a prior for the next time step until the simulation horizon T is reached. The resulting PDF $f_{x_{\text{leak}}|h_{\text{obs}}}(X)$ is expected to be much more narrow than the initial uninformed (i.e., uniform) prior PDF. It allows one to predict the leak location with a given/required degree of certainty.

This strategy can be augmented as follows. If the leak location is known but its strength is uncertain, then $f_{x_{\text{leak}}}$ is replaced with $f_{C_L A_L}$. If both leak location and its strength are unknown, then $f_{x_{\text{leak}}}$ is replaced with $f_{C_L A_L, x_{\text{leak}}}$ which, under the reasonable assumption of statistical independence between the leaks location and strength, becomes $f_{C_L A_L, x_{\text{leak}}} = f_{C_L A_L} f_{x_{\text{leak}}}$.

3.5 Simulation Results

In the simulations reported below, we consider a pipe of length $L = 3000$ m and diameter $D = 0.5$ m. The Darcy-Weisbach friction factor is set to $f = 0.03$. A transient wave with speed $a = 1403$ m/s is initiated by instantaneous closure of the valve at the downstream of the pipe ($x = L$). The pipe inlet ($x = 0$) has a constant pressure head of $H_{\text{in}} = 150$ m. A sensor is located at $x^\star = L/3 = 1000$ m to measure the response of the pressure head. The time required for the contact discontinuity to travel from the valve back to the inlet is $\tau = L/a = 2.14$ s, and the time required for it to reach the sensor point is $\tau^\star = (L - x^\star)/a = 1.43$ s (see Fig. 3.1). The simulation time is set to $T = 2\tau$ in order to cover two contact discontinuities passing through the sensor. If the leak is located at point $x = x_{\text{leak}}$, then the time needed for the contact discontinuity to reach it is $\tau_{\text{leak}} = (L - x_{\text{leak}})/a$.

Synthetic data $h_{\text{obs}}(t)$ are generated as follows. For a given leak location and strength, and for a known initial velocity chosen randomly from its distribution, the WHE (3.1) and (3.2) are solved to obtain the "exact" solutions $u(x,t)$ and $h(x,t)$. The pressure time series $h^\star(t) \equiv h(x^\star, t)$

is assumed to be available only at the sensor location $x^\star$. Finally, the data $h_{\text{obs}}(t)$ are generated with (3.3) in which the variance of the zero-mean white noise $\xi(t)$ is set to $\sigma_\xi^2 = 1$ to account for measurement errors and ambient noise. This gives a Gaussian observation model with mean $h_{\text{obs}}(t)$ and variance 1.

We consider three scenarios. In the first, the leak location is unknown while its strength is certain; in the second, the leak location is certain while its strength is unknown; and in the third, both the leak location and strength are unknown. In all cases, the pipe is sub-divided into $N = 120$ equal segments. The uncertain initial velocity u_0 is modeled as a lognormal random variable such that $u_0 = 2.0 + 0.1\exp(z)$, where z is a Gaussian random variable with mean $\mu_z = 0$ and standard deviation $\sigma_z = 0.4$. In all cases, the prior PDF $f_{h|x_{\text{leak}}}$ is computed by solving (3.4) and (3.5).

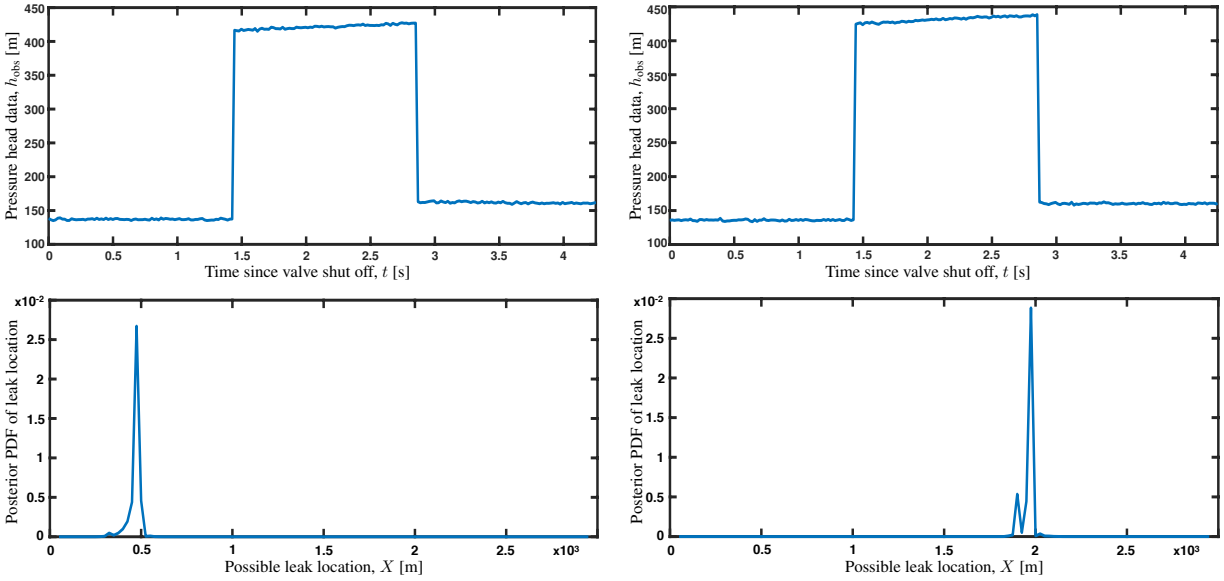

Figure 3.2: Scenario 1: Unknown leak location x_{leak} and known leak strength $C_L A_L = 10^{-4}$ m^2. The top row exhibits the sensor's pressure head readings, $h_{\text{obs}}(t)$, for a leak located either upstream of the sensor, at $x_{\text{leak}} = 475$ m (left column), or downstream, at $x_{\text{leak}} = 1975$ m (right column). The bottom row depicts the posterior PDFs $f_{x_{\text{leak}}|h_{\text{obs}}}(X)$ for these two cases.

Scenario 1: The leak strength is known, $C_L A_L = 10^{-4}$ m^2, and the unknown leak location x_{leak} is uniformly distributed in $(0, L)$. More specifically, since the simulation domain is discretized with 120 segments (121 nodes), the leak can be in any of 117 internal nodes (i.e.,

excluding two nodes from each edge) with equal probability $\mathbb{P} = 1/117$. Figure 3.2 (top row) exhibits the sensor's pressure head readings, $h_{\text{obs}}(t)$, for a leak located either upstream of the sensor, at $x_{\text{leak}} = 475$ m (left column) with $u_0 = 2.066$ m/s, or downstream, at $x_{\text{leak}} = 1975$ m (right column) with $u_0 = 2.152$ m/s. The two time series are virtually indistinguishable, with the leak discharge of about 1% of the initial flow rate in steady-state conditions. Yet our Bayesian updating procedure is capable of identifying the leak location from these data (Fig. 3.2, bottom row). During the update, the uninformative prior PDF $f_{x_{\text{leak}}}$ has been replaced with sharply peaked posterior PDFs $f_{x_{\text{leak}}|h_{\text{obs}}}$. In the case of $x_{\text{leak}} = 475$ m, the posterior PDF has the mean $\bar{x}_{\text{leak}} = 467.2$ m and, with the 95% confidence, places the leak between 402 m and 525 m. In the case of $x_{\text{leak}} = 1975$ m, the posterior PDF has the mean $\bar{x}_{\text{leak}} = 1961.7$ m and, with the 95% confidence, places the leak between 1886.4 m and 2000 m. Although not shown here, we found the width of the posterior PDF $f_{x_{\text{leak}}|h_{\text{obs}}}$, i.e., uncertainty in the estimation of the leak location, to increase as the leak strength becomes smaller and/or the measurement noise increases. This intuitive finding serves as a consistency check for the proposed approach.

Scenario 2: The leak location is known, $x_{\text{leak}} = 2475$ m, and the unknown leak strength $C_L A_L$ is uniformly distributed between 10^{-5} m^2 and 10^{-3} m^2. The pressure head response at the sensor, $h_{\text{obs}}(t)$, for the (unknown) leak strength $C_L A_L = 5 \cdot 10^{-5}$ m^2 with $u_0 = 2.104$ m/s is shown in Figure 3.3, together with the posterior PDF $f_{C_L A_L|h_{\text{obs}}}(\mathcal{A})$ used to estimate the leak strength from pressure measurement. This PDF has the mean $\overline{C_L A_L} = 4.1 \cdot 10^{-5}$ m^2 and, with the 95% confidence, predicts the leak strength $C_L A_L$ to lie between $2.7 \cdot 10^{-5}$ m^2 and $6 \cdot 10^{-5}$ m^2.Although not shown here, we found the performance of our method in this scenario to be sensitive to the degree of uncertainty in the initial velocity u_0. If a guessed value of u_0 is far from the mean $\bar{u}_0$, then the posterior PDF of the leak strength is centered around an erroneous value of $\overline{C_L A_L}$.

Scenario 3: Both leak location x_{leak} and its strength $C_L A_L$ are unknown. The prior PDF $f_{x_{\text{leak}}}(X)$ is uniform on the 117 internal nodes; the prior PDF $f_{C_L A_L}(\mathcal{A})$ is uniform on the interval $[10^{-5}\text{ m}^2, 10^{-3}\text{ m}^2]$. The pressure head response at the sensor, $h_{\text{obs}}(t)$, for the (unknown) leak

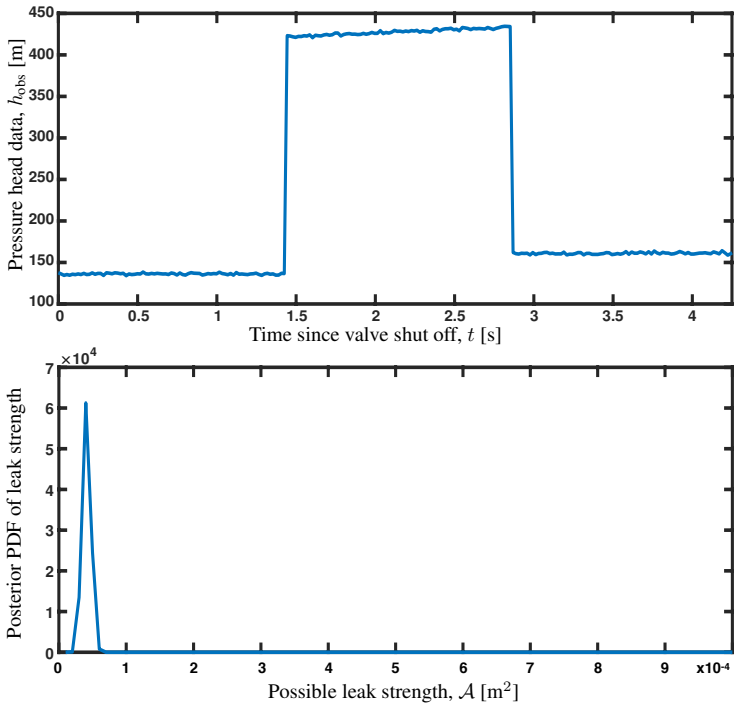

Figure 3.3: Scenario 2: Known leak location $x_{\text{leak}} = 2475$ m and unknown leak strength $C_L A_L$. The top figure exhibits the sensor's pressure head readings, $h_{\text{obs}}(t)$, for the leak strength $C_L A_L = 5 \cdot 10^{-5}$ m^2. The bottom figure exhibits the posterior PDFs $f_{C_L A_L | h_{\text{obs}}}(\mathcal{A})$.

location $x_{\text{leak}} = 1975$ m and the (unknown) leak strength $C_L A_L = 10^{-4}$ m^2 with $u_0 = 2.091$ m/s is shown in Figure 3.4, together with the posterior PDFs $f_{x_{\text{leak}}|h_{\text{obs}}}(X)$ and $f_{C_L A_L|h_{\text{obs}}}(\mathcal{A})$ used to estimate, respectively, the leak location and strength from pressure measurement. Even in the presence of two sources of uncertainty, Bayesian updating is capable of accurate leak identification. The posterior PDF $f_{x_{\text{leak}}|h_{\text{obs}}}$ has the mean $\bar{x}_{\text{leak}} = 1995.5$ m and, with the 95% confidence, places the leak between 1950 m and 2045 m. The posterior PDF $f_{C_L A_L|h_{\text{obs}}}$ has the mean $\overline{C_L A_L} = 10^{-4}$ m^2 and, with the 95% confidence, predicts the leak strength $C_L A_L$ to lie between $9 \cdot 10^{-5}$ m^2 and $1.2 \cdot 10^{-4}$ m^2. In other words, the means of these distributions provide accurate estimates of both the location and strength of the leak, but predictive uncertainty associated with these estimators increases relative to Scenarios 1 and 2.

The results reported above show that Bayesian data assimilation, combined with the method of distributions, is powerful tool for detection of small leaks in the presence of uncertain conditions and ambient noise. Bayesian updating produces a posterior PDFs for non-Gaussian nonlinear models. The results are accurate even for small leaks with uncertain initial velocity and errors in sensor reading.

3.6 Conclusions

We introduces an approach, which combines Bayesian data assimilation with the method of distributions, for leak detection in water pipes instrumented with pressure sensors. The method of distributions provides a deterministic linear equation for the PDF of pressure head, whose dynamics is described by (highly nonlinear) water hammer equations; this significantly reduces the computational cost relative to Monte Carlo simulations of the water hammer equations. A solution of this PDF equation serves as a prior distribution in the Bayes formula. We conducted a series of numerical experiments to demonstrate the applicability of our approach to pipe flows with uncertain initial velocity and ambient noise.

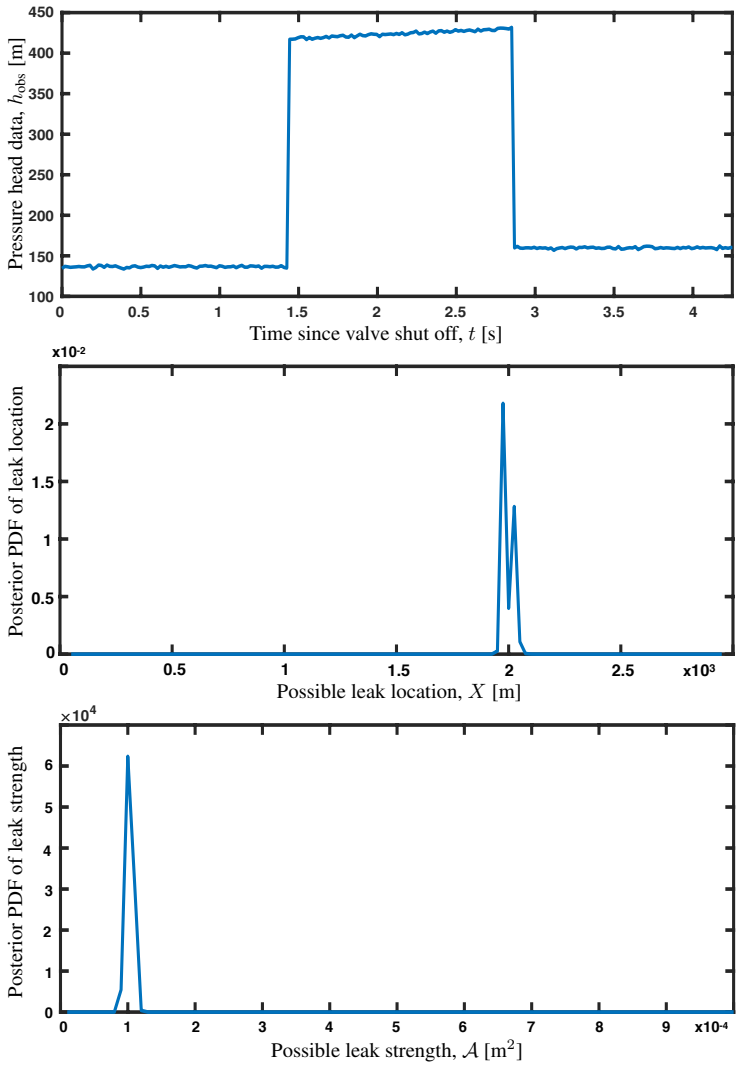

Figure 3.4: Scenario 3: Both leak location x_{leak} and its strength $C_L A_L$ are unknown. The top figure exhibits the sensor's pressure head readings, $h_{\text{obs}}(t)$, for the leak location $x_{\text{leak}} = 1975$ m and strength $C_L A_L = 10^{-4}$ m^2. The remaining two figures depict the posterior PDFs of the leak location, $f_{x_{\text{leak}}|h_{\text{obs}}}(X)$, and leak strength, $f_{C_L A_L|h_{\text{obs}}}(\mathcal{A})$.

Unlike various flavors of Kalman filter, Bayesian updating does not require a system to be linear or Gaussian; that is particular pertinent for highly nonlinear water hammer equations whose solutions exhibit multiple discontinuities. Our numerical experiments demonstrated how uninformed priors, which reflect the lack of knowledge about a leak's location and strength, transform themselves into sharp posterior distributions centered around the actual values of the leak's location and strength. This was done for fairly small leaks, which are characteristic of initial stages of pipe bursts.

The width of the posterior PDFs, i.e., uncertainty in the estimation of the leak location, to increase as the leak strength becomes smaller and/or the measurement noise increases. This intuitive finding serves as a consistency check for the proposed approach.

3.7 Acknowledgments

Chapter 3, in full, has been submitted for publication of the material as it may appear in Bayesian Updating and Method of Distributions: Application to Leak Detection in Pipes. Alawadhi, A.; and Tartakovsky, D.M., Water Resource Research, 2019. The dissertation/thesis author was the primary investigator and author of this paper.

4 Leak Detection in Networks via Bayesian Update of the Method of Distributions

4.1 Introduction

Pipe networks provide a safe and economical way to deliver a fluid from its source to a desired location. They consist of many pipes connected to each other with fittings. As networks age, their pipes and fittings develop undesired abnormalities, such as leakage and contamination build up, due to increased susceptibility to erosion and corrosion. These abnormalities increase the economic and environmental costs of operating a fluid distribution network. For example, American Society of Civil Engineers estimates that around 240,000 water mains break in the United States each year (ASCE 2015); and close to 1500 major buried gas pipeline incidents have been detected in the last forty years in Europe (Guo et al. 2018).

Since visual inspection is not an option for underground fluid distribution networks, one has to rely on indirect measurements of hydraulic characteristics (e.g., pressure sensors) to identify leak locations. (A practical approach based on the mass balance between the amounts of fluid put in at the source and extracted at the end points works only when leaks are sufficiently large and does not pinpoint their locations.) Leak detection tests induce pressure transients (e.g., by shutting off a valve in one of the pipes), which carry information about a leak to the sensor in a pipe network. These so-called transient test-based techniques (TTBTs) can be grouped into the frequency domain approach (Mpesha et al. 2001, Lee et al. 2005, Covas et al. 2005), direct transient approach (Brunone 1999, Brunone & Ferrante 2001, Wang et al. 2002), and inverse transient analysis (ITA) approach (Liggett & Chen 1994, Vítkovskỳ et al. 2000, 2007, Covas & Ramos 2010, Soares et al. 2011). An extensive review of these approaches can be found in Colombo et al. (2009). Most of these approaches give accurate results for a single pipe, but have hard time dealing with networks due to the associated uncertainty and flow complexity. With some caveats, the ITA is capable of locating leaks in controlled pipe networks; yet its performance in real pipe networks is less reliable (Covas & Ramos 2010, Meniconi et al. 2015) .

Accounting for uncertainty in input parameters and operating conditions, i.e., treating

the underlying transient flow equations as stochastic, has a potential to overcome the limitations of the approaches mentioned above (Zhang et al. 2011, Duan 2015, Massari et al. 2014, Sattar & El-Beltagy 2016, Ye & Fenner 2010). Solutions of such stochastic equations are given in terms of the probability density function (PDF) f_h of pressure head h. This strategy provides a natural venue for assimilating pressure head measurements by means of either (various flavors of) Kalman filter or the Bayesian update [*ibid*]. The latter strategy does not assume that the PDF of pressure head is Gaussian, which is a poor assumption when fluid flow obeys the water hammer equations (WHE) (Alawadhi et al. 2018). A major downside of Bayesian updating (Wikle & Berliner 2007) is its computational cost, because computation (e.g., with Monte Carlo simulations) of a full PDF used in Bayesian data assimilation is typically orders of magnitude more expensive than computation of the corresponding mean and (co)variance needed by Kalman filter.

To alleviate the computational burden of Monte Carlo computation of the PDF of pressure head, whose dynamics is described by the WHE with uncertain (random) coefficients, Alawadhi et al. (2018) used the method of distributions (Tartakovsky & Gremaud 2015) to derive a single deterministic partial differential equation (PDE) for f_h. Using the solution of this PDE as a prior distribution, and using Bayesian update to assimilate hydraulic head measurements, i.e., to compute a posterior distribution, Alawadhi & Tartakovsky (2019) identified both the location and strength of a leak in a single pipe.

In this paper, we build upon these results to develop a computationally efficient methodology for identification of leaks in a network of pipes. Section 4.2 provides a problem formulation of fluid flow in a network, which involves the WHE with random initial velocity. In section 4.3, we present equations used to obtain the PDF of the pressure head, f_h, via the method of distributions. This PDF is then used in section 4.4 as a prior for Bayesian assimilation of pressure sensor measurements. In section 4.5, we present results of our numerical experiments, which demonstrate our method's ability to localize leaks in pipe networks. This section also provides a comparison

of our method's performance with that of the commonly used "best fitness function" method of inverse transient analysis. Finally, major conclusions drawn from this study are summarized in Section 4.6.

4.2 Problem Formulation

A transient leak detection test is conducted by shutting off a valve in a pipe and taking pressure measurements from a sensor located upstream from the valve. Fluid flow induced by this procedure is described by the WHE (Chaudhry 2013, Wylie et al. 1993),

$$\frac{\partial h}{\partial t} + \frac{a^2}{g}\frac{\partial u}{\partial x} = \frac{Q_{\text{leak}}}{A}\delta(x - x_{\text{leak}}) \tag{4.1a}$$

$$\frac{\partial u}{\partial t} + g\frac{\partial h}{\partial x} = k|u|u, \qquad k = -\frac{f}{2D}, \tag{4.1b}$$

where $h(x,t)$ and $u(x,t)$ are the cross-sectionally averaged pressure head and flow velocity, respectively; g is the gravitational acceleration constant; a is the wave speed; f is Darcy-Weisbach friction factor; $A = \pi D^2/4$ is the cross-sectional area of the pipe; x_{leak} is the location of a possible leak; Q_{leak} is the intensity of the leak; and $\delta(\cdot)$ is the Dirac delta function which represents the leak as a point source/sink. These equations are obtained by averaging Naiver-Stokes equation in a pipe over the pipe's cross-section.

The WHE (4.1) are subject to initial and boundary conditions, which reflect a pipe network's topology. We consider scenarios in which the pressure head at the inlet of the pipe containing a pressure sensor is known, $h(0,t) = H_{\text{in}}$, while flow velocity at the outlet is $u = 0$ after the valve's shut off ($t > 0$). The initial conditions are obtained from the steady-state flow before the valve's shut off. This gives a constant initial velocity u_0 along the length of the instrumented pipe. The corresponding initial pressure varies spatially, $h_0(x;u_0) = (k/g)|u_0|u_0 x + H_{\text{in}}$, in accordance with the steady-state WHE.

The intersecting pipes are assumed to have the same pressure head at junction nodes, while the velocities are related to each other by continuity equation

$$\sum_{i}^{N_{\text{in}}} Q_{\text{in}_i} = \sum_{i}^{N_{\text{out}}} Q_{\text{out}_i} \tag{4.2}$$

where Q_{in} and Q_{out} are the flow rates entering the junction node and exiting the junction node, respectively. The same reasoning applied to the leak location $x = x_{\text{leak}}$ suggests the equality of the pressure head immediately upstream and downstream of the leak, $h(x^{-}_{\text{leak}},t) = h(x^{+}_{\text{leak}},t) = h(x_{\text{leak}},t)$. The velocities at this point are related by mass conservation (Brunone 1999),

$$Q^{-} = Q^{+} + Q_{\text{leak}}, \qquad Q_{\text{leak}}(t) = C_L A_L \sqrt{2gh(x = x_{\text{leak}},t)}, \tag{4.3}$$

where Q^{-} and Q^{+} are the upstream flow rate and the downstream flow rate, respectively; C_L is the discharge coefficient; and A_L is the leak area. The product $C_L A_L$ is referred to as the strength of the leak.

The location (x_{leak}) and strength ($C_L A_L$) of the leak and the initial flow velocity (u_0) are all unknown. They are treated as random variables with prescribed PDFs. The initial velocity is assigned a PDF f_{u_0}. The PDF of the leak location, $f_{x_{\text{leak}}}$ and the PDF of the strength of the leak, $f_{C_L A_L}$, are a priori assigned uniform distributions on the intervals $[\mathcal{X}_{min}, \mathcal{X}_{max}]$ and $[\mathcal{A}_{min}, \mathcal{A}_{max}]$, respectively. Within the Bayesian framework, such PDFs are referred to as uninformative priors and reflect no prior knowledge of the leak.

Measurements are collected by a pressure sensor located in one of the pipes at a point $x = x^{\star}$. Measurement errors are accounted for by adding zero-mean Gaussian white noise, $\xi(t)$, to obtain the model for pressure sensor readings, $h_{\text{obs}}(t)$,

$$h_{\text{obs}}(t) = h(x^{\star},t) + \xi(t). \tag{4.4}$$

This formulation implicitly assumes that the WHE provides an accurate representation of reality, i.e., that the model's prediction $h(x^\star,t)$ differs from the measurements at the same point, $h_{\text{obs}}(t)$, only by measurement error.

The prior PDF of the pressure head, $f_h(H;x,t)$, can be computed with high-resolution Monte Carlo simulations of the WHE (4.1), which is computationally expensive and often prohibitively so. Instead, we compute it by solving the PDF equation introduce in the following section.

4.3 Method of Distributions

Applying the method of distributions (Tartakovsky & Gremaud 2015) to the WHE (4.1), one obtains a deterministic equation for the PDF, $f_h(H;x,t)$, of the pressure head $h(x,t)$ (Alawadhi et al. 2018):

$$\frac{\partial f_h}{\partial t}+\frac{\partial V f_h}{\partial H}=0, \qquad V=-\frac{a^2}{g}\frac{\partial \bar{u}}{\partial x}+\frac{Q_{\text{leak}}}{A}\delta(x-x_{\text{leak}})-\alpha_1(H-\bar{h}). \tag{4.5a}$$

This linear equation, which is valid at space-time intervals between the pressure discontinuities (see below), implies that the PDF f_h is advected in the two-dimensional space (x,H) by the velocity field $V(h,H,t)$ that is aligned with the H coordinate. The velocity field depends on the ensemble mean velocity, $\bar{u}(x,t)$, and ensemble mean pressure head, $\bar{h}(x,t)$. It also depends on the variance of the pressure head, $\sigma_h^2(x,t)$, through the closure variable α_1, which is given by

$$\alpha_1=-\frac{C_L A_L\sqrt{2g}\delta\left(x-x_{\text{leak}}\right)}{2A\sqrt{\bar{h}}}+\frac{1}{2}\frac{\partial \ln\sigma_h^2}{\partial t}. \tag{4.5b}$$

The PDF equation (4.5) is subject to initial and boundary conditions that reflects the information about the initial and boundary conditions of the physical system. This is done by numerically relating the pressure head after the ith discontinuity, h_i ($i=1,2,\cdots$), to the initial

velocity, u_0. The relation $h_i = h_i(u_0)$ is obtained by solving the WHE (4.1) with the method of characteristics N times, each with a different realization of u_0, to obtain the pressure head after the ith discontinuity, h_i. This procedure results in a data array $\{u_0^{(k)}, h_i^{(k)}\}_{k=1}^{N}$, which is then fitted with a second-order polynomial, $u_0 = \alpha_i h_i^2 + \beta_i h_i + \gamma_i$. The coefficients α_i, β_i, and γ_i are obtained through minimization of mean root square error between the data and this polynomial. Finally, the PDF of the pressure head after each discontinuity is computed as

$$f_{h_i} = \left| \frac{\mathrm{d}u_0}{\mathrm{d}h_i} \right| f_{u_0}. \tag{4.6}$$

The PDF equation (4.5) is solved multiple times for each leak candidate (location/strength) to obtain a conditional PDF for the pressure head, $f_{h|x_{\text{leak}},C_LA_L}(H;x^\star,t)$, which is used for data assimilation. It only needs to be solved for the sensor node $x = x^\star$, since the physical space coordinate x is a parameter in the equation. This prior PDF is updated with the pressure head measurements using the Bayesian procedure described below.

4.4 Data Assimilation

Once the conditional PDF $f_{h|x_{\text{leak}},C_LA_L}(H;x^\star,t)$ is computed, and the leak-related priors $f_{x_{\text{leak}}}(X)$ and $f_{C_LA_L}(A)$ are assigned, the prior joint PDF $f_{h,x_{\text{leak}},C_LA_L}(H,X,A;x^\star,t)$ is evaluated as

$$f_{h,x_{\text{leak}},C_LA_L}(H,X,A;x^\star,t) = f_{h|x_{\text{leak}},C_LA_L}(H;x^\star,t) f_{x_{\text{leak}}}(X) f_{C_LA_L}(A). \tag{4.7}$$

We use Bayesian updating (Wikle & Berliner 2007) to assimilate the measurement h_{obs} at a given time t into this probabilistic prediction. For the measurement error model in (4.4), $f_{h_{\text{obs}}|h,x_{\text{leak}},C_LA_L}$,

the PDF of h_{obs} conditioned on the WHE's prediction $h(x,t)$, is Gaussian,

$$f_{h_{\text{obs}}|h,x_{\text{leak}},C_LA_L} = \frac{1}{\sqrt{2\pi\sigma_\xi^2}} \exp\left[-\frac{(H-h_{\text{obs}})^2}{2\sigma_\xi^2}\right] \tag{4.8}$$

Then, Bayes' theorem gives the posterior joint PDF,

$$f_{h,x_{\text{leak}},C_LA_L|h_{\text{obs}}} = \frac{f_{h_{\text{obs}}|h,x_{\text{leak}},C_LA_L} f_{h,x_{\text{leak}},C_LA_L}}{f_{h_{\text{obs}}}}, \tag{4.9a}$$

where $f_{h_{\text{obs}}}$ is the normalizing constant,

$$f_{h_{\text{obs}}} = \int f_{h_{\text{obs}}|h,x_{\text{leak}},C_LA_L} f_{h,x_{\text{leak}},C_LA_L} \mathrm{d}H. \tag{4.9b}$$

The posterior PDFs for leak location, $f_{x_{\text{leak}}}(X)$, and leak strength, $f_{C_LA_L}(A)$, are marginals of the posterior PDF $f_{h,x_{\text{leak}},C_LA_L|h_{\text{obs}}}$,

$$f_{x_{\text{leak}}|h_{\text{obs}}} = \int\int f_{h,x_{\text{leak}},C_LA_L|h_{\text{obs}}} \mathrm{d}H\mathrm{d}A \tag{4.10}$$

and

$$f_{C_LA_L|h_{\text{obs}}} = \int\int f_{h,x_{\text{leak}},C_LA_L|h_{\text{obs}}} \mathrm{d}H\mathrm{d}X. \tag{4.11}$$

These posterior PDFs for leak location and leak strength at time t are used as prior PDFs for the next time step. This procedure is repeated until all pressure sensor readings are assimilated. The result is the posterior PDFs $f_{x_{\text{leak}}|h_{\text{obs}}}$ and $f_{C_LA_L|h_{\text{obs}}}$ that are narrow and centered around the actual location and strength of the leak. Numerical implementation of our method follows the algorithm in Figure 4.1.

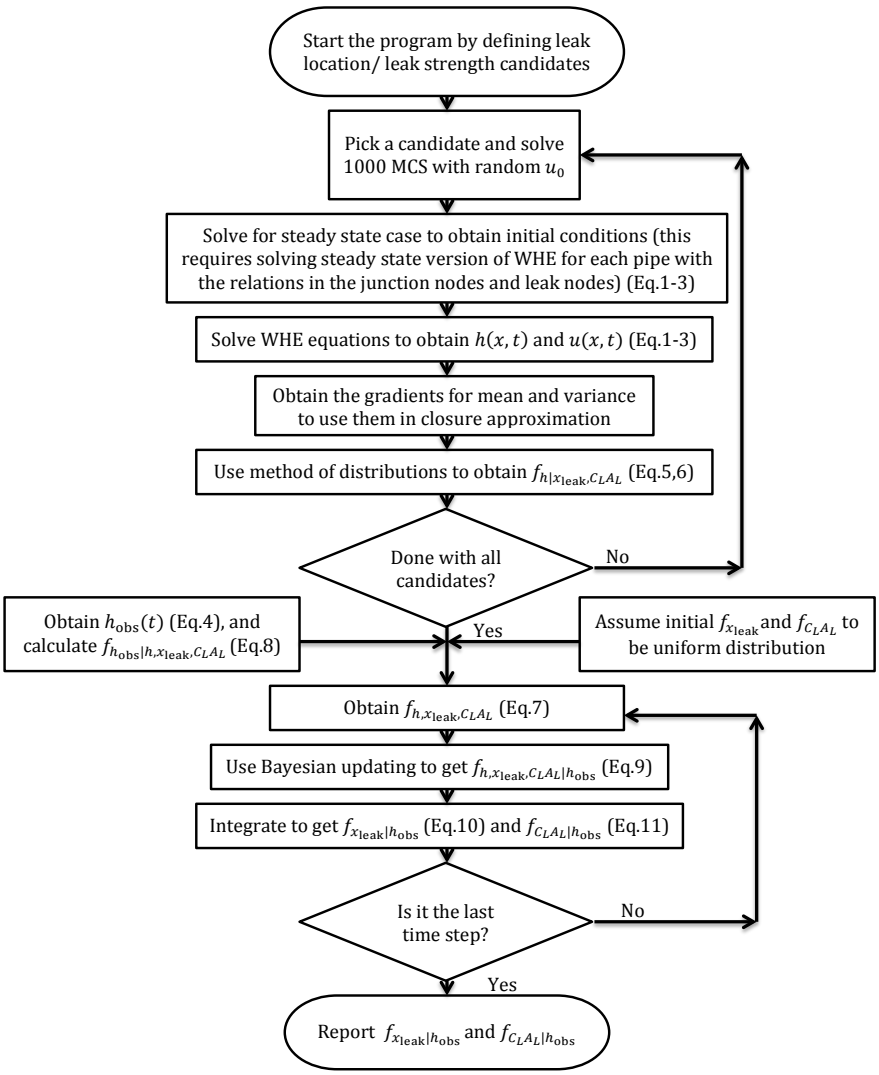

Figure 4.1: Numerical implementation of Bayesian update of the method of distribution used to locate a leak in a fluid distribution network.

4.5 Numerical Experiments

To demonstrate the ability of our method to identify leaks, we consider two pipe systems, a branching pipe and a pipe network consisting of 13 pipes.

4.5.1 Branching Pipe

As a first test, we consider a long pipe that splits into two "daughter" pipes (Fig. 4.2). The "mother" pipe is connected to a water tank in which constant and known pressure head, $H_{\text{in}} = 150$ m, is maintained; the pipe is equipped with a pressure sensor located at $x = x^\star = 1000$ m. The mother and daughter pipes have respective lengths $L_1 = 3000$ m and $L_2 = L_3 = 2000$ m, and diameter $D_1 = D_2 = D_3 = 0.5$ m. One of the daughter pipes has a dead end, while the other daughter pipe is connected to a downstream shutoff valve that is used to create transient effects by sudden closure at time $t = 0$. (The remainder of a possible pipe network downstream of the valve is immaterial for this test.) The pressure signal induced by the valve closure is captured by the sensor and used to identify leak location (x_{leak}) and intensity (Q_{leak}). A leak can be in any of the three pipes.

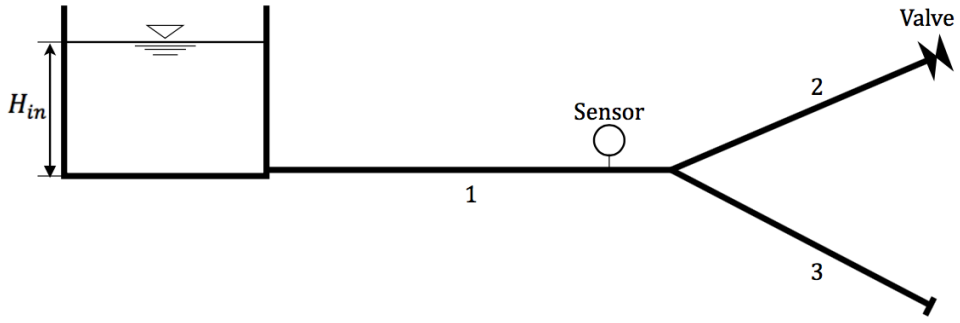

Figure 4.2: A branched pipe system used in Test I with a mother pipe connected to a tank, a daughter with a dead end, and the other daughter connected to a valve.

The flow before the valve shutoff is steady. All the pipes have the Darcy-Weisbach friction factor $f = 0.03$. The valve shutoff creates a wave traveling upstream with the wave speed whose

value is set to $a = 1403$ m/s. In numerical simulations, the pipes are discretized into equally spaced nodes with the mesh size $\mathrm{d}x = 100$ m. Absent any information, the leak can be in any of the internal nodes of the three pipes, and leak strength can be between $C_L A_L = 10^{-5}$ m^2 and $20.0 \cdot 10^{-5}$ m^2. This lack of information about the leak's location and strength is treated by assigning the uniform (uninformative) prior PDFs to both.

In this test and the one described in the following section, as well as for all scenarios considered, we treat the uncertain initial velocity u_0 as a lognormal random variable, $u_0 = 2.0 + 0.1\exp(z)$, where z is a Gaussian random variable with mean $\mu_z = 0$ and standard deviation $\sigma_z = 0.4$. Data $h_{\text{obs}}(t)$ are generated by solving the WHE (4.1) for a given leak location and strength, with a known initial velocity chosen randomly from the distribution f_{u_0}, and then adding a zero-mean white noise to the result at sensor location $x^\star$. The variance of the noise is set to $\sigma_\xi^2 = 1$ to account for ambient noise and measurement errors, which translates into the measurement errors that are up to 2.5% of the original signal in some realizations. This choice of ξ gives a Gaussian distribution for the observation model with mean $h_{\text{obs}}(t)$ and variance 1.

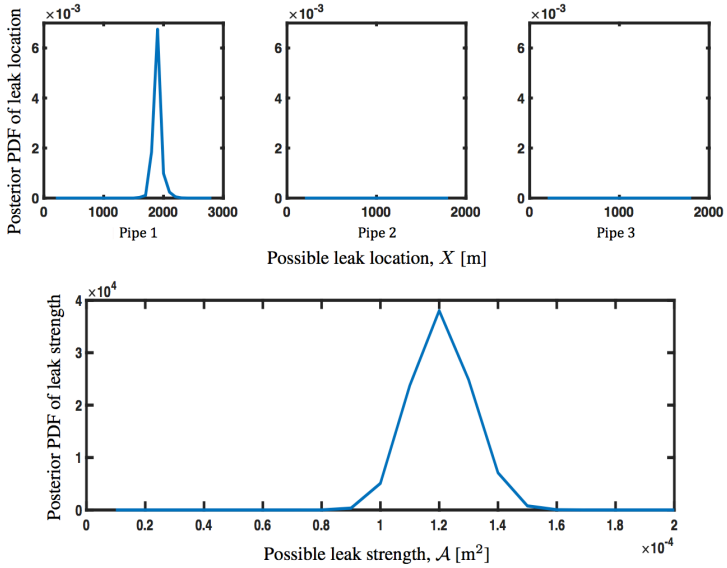

Figure 4.3: Scenario 1: Branched pipe case with a leak in pipe 1 at $x_{\text{leak}} = 1900$ m with a strength of $C_L A_L = 10.0 \cdot 10^{-5}$ m^2, where both leak location x_{leak} and its strength $C_L A_L$ are assumed unknown. The top figure depicts the posterior PDF $f_{x_{\text{leak}}|h_{\text{obs}}}(X)$. The bottom figure exhibits the posterior PDF $f_{C_L A_L|h_{\text{obs}}}(\mathcal{A})$.

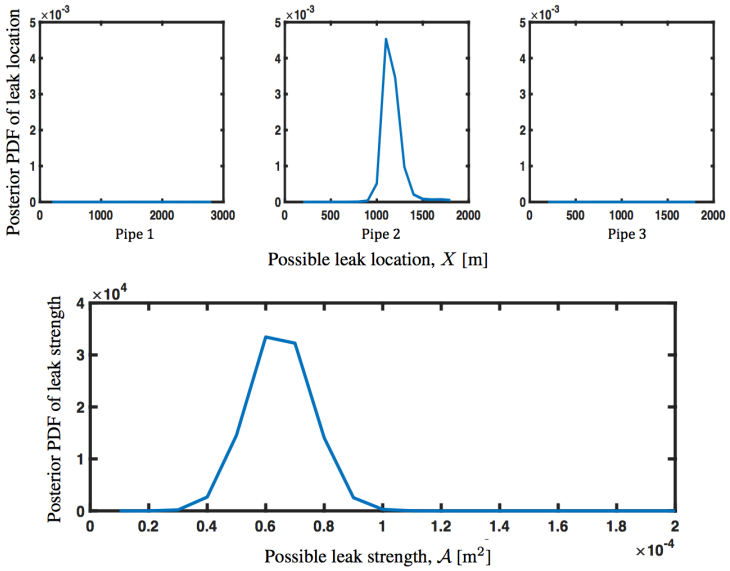

Figure 4.4: Scenario 2: Branched pipe case with a leak in pipe 2 at $x_{\text{leak}} = 1100$ m with a strength of $C_L A_L = 10.0 \cdot 10^{-5}$ m^2, where both leak location x_{leak} and its strength $C_L A_L$ are assumed unknown. The top figure depicts the posterior PDF $f_{x_{\text{leak}}|h_{\text{obs}}}(X)$. The bottom figure exhibits the posterior PDF $f_{C_L A_L|h_{\text{obs}}}(\mathcal{A})$.

We investigate our method's ability to identify a leak located in pipe 1 (scenario 1), pipe 2 (scenario 2), or pipe 3 (scenario 3). Figures 4.3–4.5 show the posterior PDF of the leak location, $f_{x_{\text{leak}}|h_{\text{obs}}}$ and the posterior PDF of the strength of the leak, $f_{C_L A_L|h_{\text{obs}}}$ for these three scenarios. Our method is capable of correctly identifying a leaky pipe in the network by transforming the uniform priors into sharper PDFs centered around the actual values for leak location and strength. The mean and the 95% confidence level computed with the posterior PDFs in Figures 4.3–4.5 are reported in Table 4.2.

4.5.2 Network of Pipes

The second test involves a network of 13 pipes, whose intersections form 7 junction nodes (Fig. 4.6). The lengths and diameters of these pipes are listed in Table 4.1. This network configuration has been used by Liggett & Chen (1994), Vítkovskỳ et al. (2000), Kapelan et al. (2003) to study their transient test-based techniques (TTBTs). The Darcy-Weisbach friction factor

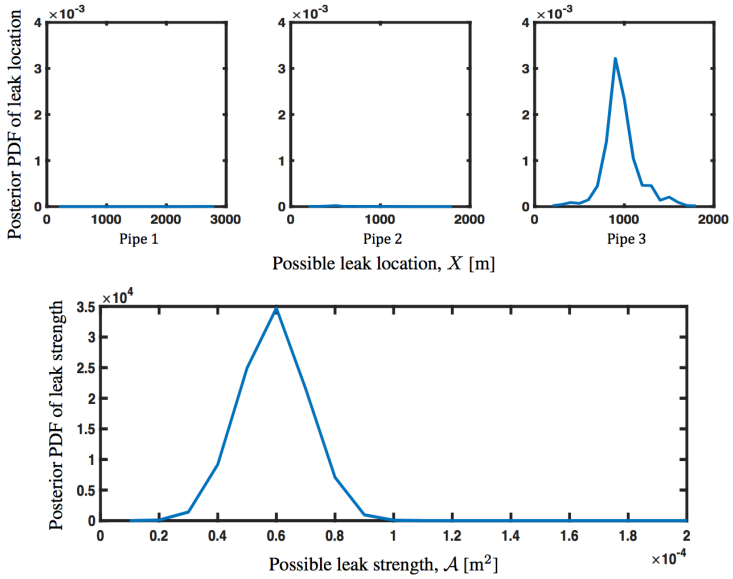

Figure 4.5: Scenario 3: Branched pipe case with a leak in pipe 3 at $x_{\text{leak}} = 800$ m with a strength of $C_L A_L = 8.0 \cdot 10^{-5}$ m^2, where both leak location x_{leak} and its strength $C_L A_L$ are assumed unknown. The top figure depicts the posterior PDF $f_{x_{\text{leak}}|h_{\text{obs}}}(X)$. The bottom figure exhibits the posterior PDF $f_{C_L A_L|h_{\text{obs}}}(\mathcal{A})$.

for all pipes is $f = 0.02$. The inlet of the network is connected to a water tank with a known pressure head, $H_{\text{in}} = 150$ m. A pressure sensor is installed on the inlet pipe at $x = x^\star$. The outlet pipe is connected to a shutoff valve that is used for water-hammer test.

The experiment starts with steady flow before the valve shutoff. Three scenarios are discussed for this test, each with its own pipe discretization and sensor location. For scenario 4, pipe 1 is equipped with a pressure sensor at $x^\star = 1750$ m and is discretized with a uniform mesh of size $\mathrm{d}x = 250$ m. All the pipes in the network (or, more precisely, their internal nodes) are treated as leak candidates, and the prior PDF for leak strength $C_L A_L$ is a uniform distribution on the interval from $5.0 \cdot 10^{-5}$ m^2 to $20.0 \cdot 10^{-5}$ m^2. The actual leak, used to generate data, is located in pipe 7 at $x_{\text{leak}} = 1000$ m (which is the 61st node) and has the intensity of $C_L A_L = 10.0 \cdot 10^{-5}$ m^2; the initial flow velocity is $u_0 = 2.110$ m/s. The posterior PDF after Bayesian updating, $f_{x_{\text{leak}}|h_{\text{obs}}}(X)$, is shown in Figure 4.7. It identifies the leak in pipe 7 with 90% confidence, and has the mean of $\bar{x}_{\text{leak}} = 1960$ m. The 95% confidence predicted the leak strength to lie between $6.8 \cdot 10^{-5}$ m^2 and

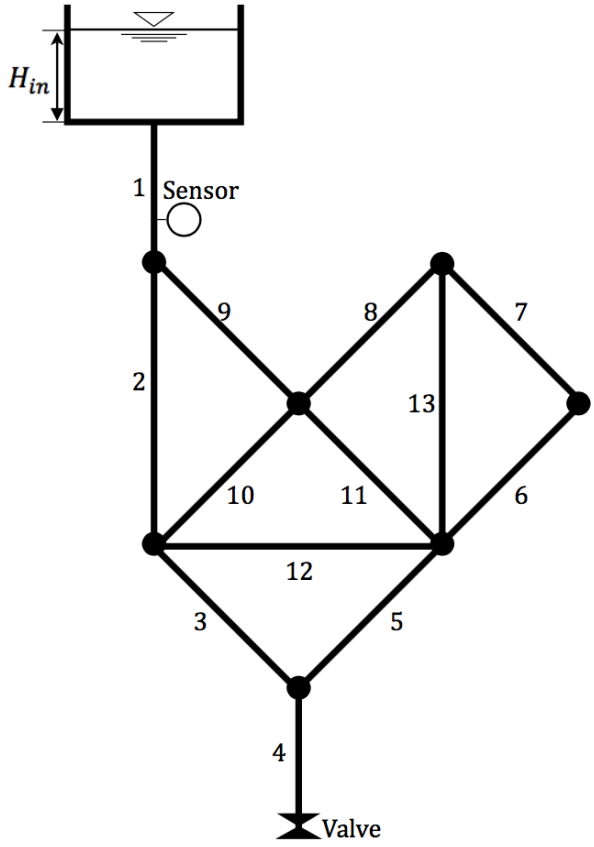

Figure 4.6: Pipe network system used in Test II with a tank connected to the inlet and a valve connected to the outlet.

$15.0 \cdot 10^{-5}$ m^2, with the mean of $\overline{C_L A_L} = 10.5 \cdot 10^{-5}$ m^2.

Table 4.1: Lengths and diameters of pipes in the pipe network system used in the last three scenarios.

	Length (m)	Diameter (m)
Pipe 1	3000	0.5
Pipe 2	4000	0.4
Pipe 3	3000	0.4
Pipe 4	3000	0.5
Pipe 5	3000	0.4
Pipe 6	3000	0.3
Pipe 7	3000	0.25
Pipe 8	2500	0.25
Pipe 9	2500	0.4
Pipe 10	2500	0.3
Pipe 11	2500	0.4
Pipe 12	3000	0.3
Pipe 13	4000	0.4

We used the previous scenario to demonstrate the method's ability to locate the leaky pipe; in doing so, a coarse numerical mesh was used to speed up the computations. The next two scenarios refine the computational mesh to pinpoint the leak location within the leaky pipe (identified, e.g., by using the coarse mesh of scenario 4). This strategy reduces the computation time by searching for the leak candidates on the refined mesh only in a leaky pipe. In scenario 5 the sensor is placed in pipe 1 at $x^\star = 2000$ m, and this pipe is discretized with a finer mesh of size $\mathrm{d}x = 100$ m. In this scenario, pipe 9 is known to be leaking, but the exact leak location is unknown and treated as a random variable uniformly distributed between 200 m and 2300 m. The leak strength is also unknown and treated as a uniform random variable on the interval between $2.0 \cdot 10^{-5}$ m^2 and $14.0 \cdot 10^{-5}$ m^2. The actual leak used in this test is at $x_{\text{leak}} = 1400$ m and has the strength $C_L A_L = 10.0 \cdot 10^{-5}$ m^2; the initial flow velocity is $u_0 = 2.102$ m/s. Our method predicts the mean for leak location at $\bar{x}_{\text{leak}} = 1426$ m; with 95% confidence it places the leak between

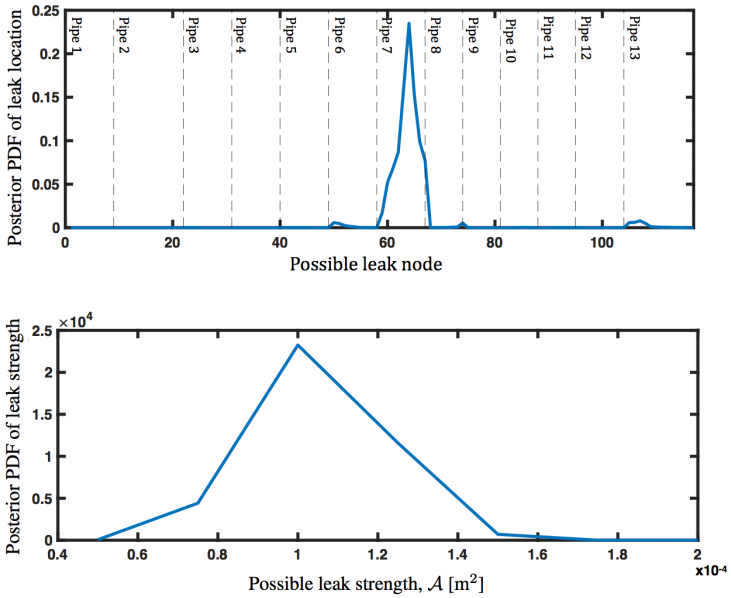

Figure 4.7: Scenario 4: Pipe network case with a leak in pipe 7 at $x_{\text{leak}} = 1000$ m with a strength of $C_L A_L = 10.0 \cdot 10^{-5}$ m^2, where both leak location x_{leak} and its strength $C_L A_L$ are assumed unknown. The top figure depicts the posterior PDF $f_{x_{\text{leak}}|h_{\text{obs}}}(X)$. The bottom figure exhibits the posterior PDF $f_{C_L A_L|h_{\text{obs}}}(\mathcal{A})$.

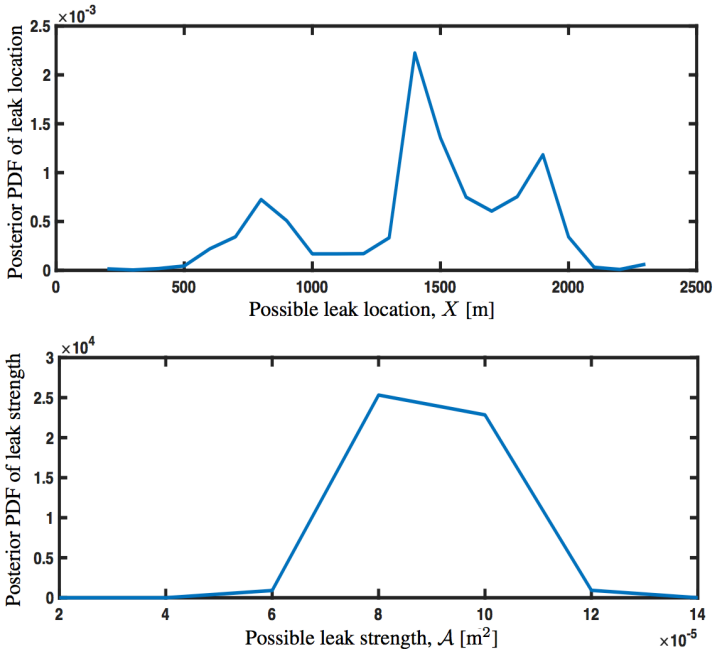

Figure 4.8: Scenario 5: Pipe network case with a leak in pipe 9 at $x_{\text{leak}} = 1400$ m with a strength of $C_L A_L = 10.0 \cdot 10^{-5}$ m^2, where both leak location x_{leak} and its strength $C_L A_L$ are assumed unknown. The top figure depicts the posterior PDF $f_{x_{\text{leak}}|h_{\text{obs}}}(X)$. The bottom figure exhibits the posterior PDF $f_{C_L A_L|h_{\text{obs}}}(\mathcal{A})$.

600 m and 1991 m. The predicted mean for the leak strength is $\overline{C_L A_L} = 9.0 \cdot 10^{-5}$ m^2; with 95% confidence the leak strength is between $6.0 \cdot 10^{-5}$ m^2 and $11.7 \cdot 10^{-5}$ m^2 (Fig. 4.8).

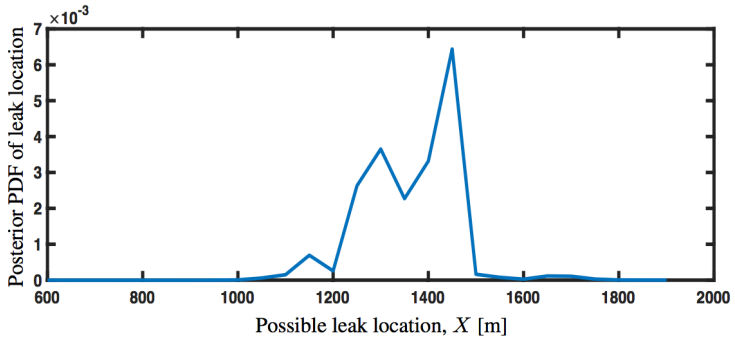

Figure 4.9: Scenario 6: posterior PDF $f_{x_{\text{leak}}|h_{\text{obs}}}(X)$ for pipe network case with a leak in pipe 10 at $x_{\text{leak}} = 1450$ m with a strength of $C_L A_L = 10.0 \cdot 10^{-5}$ m^2, where leak location x_{leak} is assumed unknown and leak strength $C_L A_L$ is known.

The last scenario has a sensor in pipe 1 at $x^\star = 1000$ m, which is discretized with a very fine mesh of size d$x = 50$ m. The leak is known to be in pipe 10 with unknown exact location, a situation modeled by treating x_{leak} as a uniformly distributed random variable on the interval between 600 m and 1900 m. The leak size is assumed to be known, $C_L A_L = 10.0 \cdot 10^{-5}$ m^2. The actual leak used to generate data is at $x_{\text{leak}} = 1450$ m, and the initial flow velocity is $u_0 = 2.091$ m/s. Our method places the mean of leak location at $\bar{x}_{\text{leak}} = 1363$ m; with 95% confidence, the leak is located between 1149 m and 1500 m (Fig. 4.9).

4.5.3 Comparison with an Alternative Method

We compare the performance of our Bayesian method with that of the commonly used inverse transient analysis method based on a "best fitness function". The fitness function is defined as the discrepancy between the observed and predicted pressure heads,

$$\mathcal{F}(u_0, x_{\text{leak}}, C_L A_L) = \sum_{t=i\cdot dt}^{T_{\max}} |h_{\text{obs}}(t) - h(x^\star, t; x_{\text{leak}}, C_L A_L)|, \qquad i = 0, 1, 2 \cdots T_{\max}/dt$$

and the "best" refers to a solution of the minimization problem

$$\{\hat{x}_{\text{leak}}, \widehat{C_L A_L}\} = \underset{u_0, x_{\text{leak}}, C_L A_L}{\operatorname{argmin}} \mathcal{F}(u_0, x_{\text{leak}}, C_L A_L).$$

In its standard formulation, all the quantities in the best fitness function are deterministic, i.e., uncertainty in the input parameters and measurement errors are ignored.

Table 4.2: A comparison between the actual values, values obtained with Bayesian updating, and values obtained using best fitness function for the branched pipe case results.

	Actual			Bayesian updating		Best fitness	
	u_0 (m/s)	x_{leak} (m)	$C_L A_L$ (10^{-5}m^2)	x_{leak} (m) (95% CL)	$C_L A_L$ (10^{-5}m^2) (95% CL)	x_{leak} (m)	$C_L A_L$ (10^{-5}m^2)
Scenario 1	2.082	1900	10.0	1895 (1725-2100)	12.1 (9.2-14.0)	1900	14.0
Scenario 2	2.120	1100	10.0	1167 (933-1400)	6.5 (4.2-9.0)	1100	8.0
Scenario 3	2.109	800	8.0	948 (600-1560)	5.9 (3.0-8.1)	900	6.0

The result using the best fitness function is reported in Table 4.2 for the branched pipe case. For scenario 4, the method was able to locate the leak in the correct pipe with $x_{\text{leak}} =$ 1750 m and $C_L A_L = 15.0 \cdot 10^{-5}$ m^2. It predicted the leak at $x_{\text{leak}} = 600$ m with a strength of $C_L A_L = 8.0 \cdot 10^{-5}$ m^2 for scenario 5, and predicted the leak at $x_{\text{leak}} = 1300$ m for scenario 6. Both the best fitness function and our method correctly pick a leaky pipe in the networks, and their respective accuracy in terms of the leak's location and strength vary from one scenario to the next. It is important to emphasize though that our method yields predictions under uncertainty that come with corresponding confidence intervals, while the best fitness function method disregards all sources of uncertainty yielding a single (deterministic) prediction.

4.6 Conclusions

We developed a leak identification method that combines the method of distributions for the water hammer equations and Bayesian updating. The former component facilitates the efficient and accurate computation of a prior probability density function (PDF) of pressure head, while the latter allows one to update this PDF with pressure measurements collected by a sensor in one pipe of a fluid distribution network. The method of distributions transfers the nonlinear WHE with uncertain inputs into a deterministic linear equation for the PDF of pressure head. Bayesian updating was chosen for data assimilation because it allows one to handle highly non-Gaussian PDFs typical of solutions to the WHE and to make inference from noisy data in the presence of ambient noise.

Our method was applied in multiple scenarios for a bifurcating pipe and a pipe network. The results of our numerical experiments demonstrates our method's ability to correctly identify a leaky pipe for all levels of uncertainty and noise considered. It also predicted the leak's location and strength, together with the corresponding confidence intervals. The actual location and strength fell within these intervals in all experiments.

4.7 Acknowledgments

Chapter 4, in full, has been submitted for publication of the material as it may appear in Leak Detection in Networks via Bayesian Update of the Method of Distributions. Alawadhi, A.; and Tartakovsky, D.M., Water Resource Research, 2019. The dissertation/thesis author was the primary investigator and author of this paper.

5 Conclusions

A key accomplishment of this work is the derivation of a deterministic linear partial differential equation for the probability density function for fluid pressure head using the method of distributions. This equation is derived from the stochastic nonlinear water-hammer equations with uncertain initial conditions. The new approach has the ability to estimate the probability density function for pressure head and velocity in less computational cost than Monte Carlo simulations.

The obtained PDF is used as a prior distribution to locate leaks and their strength by combining it with a statistical model for pressure sensor observations using Bayesian data assimilation. We demonstrated the method's ability to obtain leak location and leak strength distributions around the actual values with acceptable accuracy. The obtained results give full distribution for the probability, which can be used to obtain higher moments and get detailed statistics about the leak. The accuracy of the results can be improved by collecting data from more than one sensor.

The method can be combined with inverse transient analysis to further improve leak identification and reduce false alarms. It can also be used to identify best locations for placement of pressure sensors and their optimal number.

The method is promising but it still needs to be tested in real complex networks. It also needs to include other types of uncertainties, such as uncertainty in parameters (friction, diameter, wave speed) and uncertainty in boundary conditions. This is possible through different closure approximations, which will lead to new sets of PDF equations.

The method can be applied to non-Newtonian fluids to cover other chemicals.

A Water Hammer Equations

A.1 Derivation of Water-Hammer Equations

A.1.1 Continuity Equation

$$\frac{\partial \rho}{\partial t} + \frac{1}{r}\frac{\partial}{\partial r}(\rho r u_r) + \frac{1}{r}\frac{\partial}{\partial \theta}(\rho u_\theta) + \frac{\partial}{\partial x}(\rho u_x) = 0 \tag{A.1}$$

assuming unidirectional, axisymmetric flow:

$$\frac{\partial \rho}{\partial t} + \frac{\partial}{\partial x}(\rho u) = 0 \tag{A.2}$$

Integrating the equation over the area and using Leibnitz rule:

the first term will be:

$$\begin{aligned}\int_0^{D/2} \frac{\partial \rho}{\partial t} 2\pi r dr &= \frac{\partial}{\partial t}\int_0^{D/2} 2\pi\rho r dr - 2\pi\rho r \frac{dr}{dt}\bigg|_{r=D/2} \\ &= \frac{\partial \bar{\rho} A}{\partial t} - 2\pi\rho r \frac{dr}{dt}\bigg|_{r=D/2}\end{aligned} \tag{A.3}$$

Where the average density, $\bar{\rho} = \frac{1}{A}\int_0^{D/2} 2\pi r \rho dr$

the second term will be:

$$\begin{aligned}\int_0^{D/2} \frac{\partial \rho u}{\partial x} 2\pi r dr &= \frac{\partial}{\partial x}\int_0^{D/2} 2\pi\rho u r dr - 2\pi\rho u r \frac{dr}{dx}\bigg|_{r=D/2} \\ &= \frac{\partial \overline{\rho u} A}{\partial x} - 2\pi\rho u r \frac{dr}{dx}\bigg|_{r=D/2}\end{aligned} \tag{A.4}$$

Where $\overline{\rho u} = \frac{1}{A}\int_0^{D/2} 2\pi r \rho u dr$

Substitue in (2):

$$\frac{\partial \bar{\rho} A}{\partial t} + \frac{\partial \overline{\rho u} A}{\partial x} - 2\pi\rho r\left(\frac{dr}{dt}\bigg|_{r=D/2} + u\frac{dr}{dx}\bigg|_{r=D/2}\right) = 0 \tag{A.5}$$

assume $\overline{\rho u} \approx \bar{\rho}\bar{u}$ and assume no leak:

$$\frac{\partial \bar{\rho} A}{\partial t} + \frac{\partial \bar{\rho}\bar{u}A}{\partial x} = 0 \tag{A.6}$$

$$A\frac{\partial \bar{\rho}}{\partial t} + \bar{\rho}\frac{\partial A}{\partial t} + \bar{\rho}A\frac{\partial \bar{u}}{\partial x} + \bar{\rho}\bar{u}\frac{\partial A}{\partial x} + \bar{u}A\frac{\partial \bar{\rho}}{\partial x} = 0 \tag{A.7}$$

$$\bar{\rho}\left(\frac{\partial A}{\partial t} + \bar{u}\frac{\partial A}{\partial x}\right) + A\left(\frac{\partial \bar{\rho}}{\partial t} + \bar{u}\frac{\partial \bar{\rho}}{\partial x}\right) + \bar{\rho}A\frac{\partial \bar{u}}{\partial x} = 0 \tag{A.8}$$

divide by $\bar{\rho}A$

$$\frac{1}{A}\frac{dA}{dt} + \frac{1}{\bar{\rho}}\frac{d\bar{\rho}}{dt} + \frac{\partial \bar{u}}{\partial x} = 0 \tag{A.9}$$

$$\frac{1}{\bar{\rho}A}\frac{d\bar{\rho}A}{dt} + \frac{\partial \bar{u}}{\partial x} = 0 \tag{A.10}$$

but $\frac{1}{\bar{\rho}A}\frac{d\bar{\rho}A}{dt} = \frac{1}{\bar{\rho}a^2}\frac{dP}{dt}$ where $a^2 = \frac{k/\rho}{1+\frac{kD}{Ee}c_1}$

$$\frac{1}{\bar{\rho}a^2}\frac{dP}{dt} + \frac{\partial \bar{u}}{\partial x} = 0 \tag{A.11}$$

$$\frac{\partial P}{\partial t} + \bar{u}\frac{\partial P}{\partial x} + \bar{\rho}a^2\frac{\partial \bar{u}}{\partial x} = 0 \tag{A.12}$$

Using Dimensionless Analysis:

Let $\hat{u} = \bar{u}/U_1$, $\hat{x} = x/L$, $\hat{P} = P/P_1 = \frac{P\zeta}{\rho_o a U_1}$, $\hat{t} = t/T = \frac{ta}{\zeta L}$

$$\frac{\rho_o a^2 U_1}{\zeta^2 L}\frac{\partial \hat{P}}{\partial \hat{t}} + \frac{\rho_o a U_1^2}{\zeta L}\hat{u}\frac{\partial \hat{P}}{\partial \hat{x}} + \bar{\rho}a^2\frac{U_1}{L}\frac{\partial \hat{u}}{\partial \hat{x}} = 0 \tag{A.13}$$

divide by $\frac{\bar{\rho}a^2U_1}{L}$ and let $M = \frac{U_1}{a} \ll 1$

$$\frac{\rho_o}{\bar{\rho}\zeta^2}\frac{\partial \hat{P}}{\partial \hat{t}} + \frac{\rho_o U_1}{\bar{\rho}\zeta a}\hat{u}\frac{\partial \hat{P}}{\partial \hat{x}} + \frac{\partial \hat{u}}{\partial \hat{x}} = 0 \tag{A.14}$$

$$\frac{\rho_o}{\bar{\rho}\zeta^2}\frac{\partial \hat{P}}{\partial \hat{t}} + \frac{\rho_o}{\bar{\rho}\zeta}M\hat{u}\frac{\partial \hat{P}}{\partial \hat{x}} + \frac{\partial \hat{u}}{\partial \hat{x}} = 0 \tag{A.15}$$

$$\frac{\rho_o}{\bar{\rho}\zeta^2}\frac{\partial \hat{P}}{\partial \hat{t}} + \frac{\partial \hat{u}}{\partial \hat{x}} = 0 \tag{A.16}$$

going back to dimensional form:

$$\frac{\partial P}{\partial t} + \bar{\rho}a^2\frac{\partial \bar{u}}{\partial x} = 0 \tag{A.17}$$

Use Piezometric Head:

$$P = \bar{\rho}g(\bar{h} - Z) \tag{A.18}$$

$$\frac{\partial P}{\partial t} = \bar{\rho}g\frac{\partial \bar{h}}{\partial t} \tag{A.19}$$

$$\bar{\rho}g\frac{\partial \bar{h}}{\partial t} + \bar{\rho}a^2\frac{\partial \bar{u}}{\partial x} = 0 \tag{A.20}$$

$$\frac{\partial \bar{h}}{\partial t} + \frac{a^2}{g}\frac{\partial \bar{u}}{\partial x} = 0 \tag{A.21}$$

A.1.2 Navier-Stokes Equation

$$\frac{\partial u_x}{\partial t} + u_r\frac{\partial u_x}{\partial r} + \frac{u_\theta}{r}\frac{\partial u_x}{\partial \theta} + u_x\frac{\partial u_x}{\partial x} = -\frac{1}{\rho}\frac{\partial P}{\partial x} + \frac{\kappa + \mu/3}{\rho}\frac{\partial}{\partial x}\left(\frac{\partial u_x}{\partial x}\right) + \nu\left(\frac{1}{r}\frac{\partial}{\partial r}\left(r\frac{\partial u_x}{\partial r}\right) + \frac{1}{r^2}\frac{\partial^2 u_x}{\partial \theta^2} + \frac{\partial^2 u_x}{\partial x^2}\right) + f_x \tag{A.22}$$

assuming unidirectional, axisymmetric flow:

$$\frac{\partial u}{\partial t}+u\frac{\partial u}{\partial x}=-\frac{1}{\rho}\frac{\partial P}{\partial x}+\frac{\kappa+4\mu/3}{\rho}\frac{\partial}{\partial x}\left(\frac{\partial u}{\partial x}\right)+\frac{\nu}{r}\frac{\partial}{\partial r}\left(r\frac{\partial u}{\partial r}\right)+f_x \tag{A.23}$$

Integrating the equation over the area and using Leibnitz rule:

the first term will be:

$$\begin{aligned}\int_0^{D/2}\frac{\partial u}{\partial t}2\pi r dr &= \frac{\partial}{\partial t}\int_0^{D/2}u2\pi r dr-2\pi r u\frac{dr}{dt}\bigg|_{r=D/2}\\ &= \frac{\partial(\bar{u}A)}{\partial t}-2\pi r u\frac{dr}{dt}\bigg|_{r=D/2}\end{aligned} \tag{A.24}$$

Where the average velocity $\bar{u}=\frac{1}{A}\int_0^{D/2}2\pi r u dr$

the second term will be:

$$\begin{aligned}\int_0^{D/2}u\frac{\partial u}{\partial x}2\pi r dr &= \int_0^{D/2}\frac{1}{2}\frac{\partial u^2}{\partial x}2\pi r dr\\ &= \frac{\partial}{\partial x}\int_0^{D/2}\frac{1}{2}u^2 2\pi r dr-\frac{1}{2}u^2 2\pi r\frac{dr}{dx}\bigg|_{r=D/2}\\ &= \frac{1}{2}\frac{\partial(\beta\bar{u}^2A)}{\partial x}-\frac{1}{2}u^2 2\pi r\frac{dr}{dx}\bigg|_{r=D/2}\end{aligned} \tag{A.25}$$

Where $\beta=\frac{1}{\bar{u}^2A}\int_0^{D/2}u^2 2\pi r dr$

Let $f(\rho)=\frac{1}{\rho}$, $f'(\rho)=-\frac{1}{\rho^2}$,$f''(\rho)=\frac{2}{\rho^3}$

using taylor approximation: $f(\rho)\approx\frac{1}{\bar{\rho}}-\frac{\rho'}{\bar{\rho}^2}+\frac{\rho'^2}{\bar{\rho}^3}+...$

the third term will be:

$$\begin{aligned}\int_0^{D/2} -\frac{1}{\rho}\frac{\partial P}{\partial x}2\pi r dr &= -\frac{\partial P}{\partial x}\int_0^{D/2}\frac{2\pi r}{\rho}dr \\ &= -\frac{\partial P}{\partial x}\left[\int_0^{D/2}\frac{2\pi r}{\bar{\rho}}dr - \int_0^{D/2}\frac{2\pi r\rho'}{\bar{\rho}^2}dr + \int_0^{D/2}\frac{2\pi r\rho'^2}{\bar{\rho}^3}dr\right] \\ &= -\frac{\partial P}{\partial x}\left[\frac{A}{\bar{\rho}} - \frac{A\overline{\rho'}}{\bar{\rho}^2} + \frac{A\overline{\rho'^2}}{\bar{\rho}^3}\right] = -\frac{\partial P}{\partial x}\frac{A}{\bar{\rho}} - \frac{\partial P}{\partial x}\frac{A\overline{\rho'^2}}{\bar{\rho}^3}\end{aligned} \tag{A.26}$$

the fourth term will be:

$$\begin{aligned}&\int_0^{D/2}\frac{\kappa+4\mu/3}{\rho}\frac{\partial}{\partial x}\left(\frac{\partial u}{\partial x}\right)2\pi r dr \\ &= \kappa+4\mu/3\left[\int_0^{D/2}\frac{1}{\bar{\rho}}\frac{\partial}{\partial x}\left(\frac{\partial u}{\partial x}\right)2\pi r dr - \int_0^{D/2}\frac{\rho'}{\bar{\rho}^2}\frac{\partial}{\partial x}\left(\frac{\partial u}{\partial x}\right)2\pi r dr + \int_0^{D/2}\frac{\rho'^2}{\bar{\rho}^3}\frac{\partial}{\partial x}\left(\frac{\partial u}{\partial x}\right)2\pi r dr\right] \\ &= \kappa+4\mu/3\left[\frac{\partial}{\partial x}\int_0^{D/2}\frac{1}{\bar{\rho}}\frac{\partial u}{\partial x}2\pi r dr - \frac{1}{\bar{\rho}}\frac{\partial u}{\partial x}2\pi r\frac{dr}{dx}\bigg|_{r=D/2} - \frac{A}{\bar{\rho}^2}\left\langle\rho'\frac{\partial^2 u}{\partial x^2}\right\rangle + \frac{A}{\bar{\rho}^3}\left\langle\rho'^2\frac{\partial^2 u}{\partial x^2}\right\rangle\right] \\ &= \kappa+4\mu/3\left[\frac{\partial^2}{\partial x^2}\int_0^{D/2}\frac{1}{\bar{\rho}}u2\pi r dr - \frac{2\pi r}{\bar{\rho}}(u+\frac{\partial u}{\partial x})\frac{dr}{dx}\bigg|_{r=D/2} - \frac{A}{\bar{\rho}^2}\left\langle\rho'\frac{\partial^2 u}{\partial x^2}\right\rangle + \frac{A}{\bar{\rho}^3}\left\langle\rho'^2\frac{\partial^2 u}{\partial x^2}\right\rangle\right] \\ &= \kappa+4\mu/3\left[\frac{1}{\bar{\rho}}\frac{\partial^2(\bar{u}A)}{\partial x^2} - \frac{2\pi r}{\bar{\rho}}(u+\frac{\partial u}{\partial x})\frac{dr}{dx}\bigg|_{r=D/2} - \frac{A}{\bar{\rho}^2}\left\langle\rho'\frac{\partial^2 u}{\partial x^2}\right\rangle + \frac{A}{\bar{\rho}^3}\left\langle\rho'^2\frac{\partial^2 u}{\partial x^2}\right\rangle\right]\end{aligned} \tag{A.27}$$

the fifth term will be:

$$\int_0^{D/2}\frac{\nu}{r}\frac{\partial}{\partial r}\left(r\frac{\partial u}{\partial r}\right)2\pi r dr = \int_0^{D/2}2\pi\nu\frac{\partial}{\partial r}\left(r\frac{\partial u}{\partial r}\right)dr = \pi D\nu\frac{\partial u}{\partial r}\bigg|_{r=D/2} \tag{A.28}$$

the sixth term will be:

$$\int_0^{D/2} f_x 2\pi r dr = A f_x \tag{A.29}$$

Substitue in (21) and assume no leak:

$$\frac{\partial(\bar{u}A)}{\partial t}+\frac{1}{2}\frac{\partial(\beta\bar{u}^2A)}{\partial x}=-\frac{\partial P}{\partial x}\frac{A}{\bar{\rho}}-\frac{\partial P}{\partial x}\frac{A\overline{\rho'^2}}{\bar{\rho}^3}$$
$$+(\kappa+4\mu/3)\left[\frac{1}{\bar{\rho}}\frac{\partial^2(\bar{u}A)}{\partial x^2}-\frac{1}{\bar{\rho}^2}A\left\langle\rho'\frac{\partial^2 u}{\partial x^2}\right\rangle+\frac{1}{\bar{\rho}^3}A\left\langle\rho'^2\frac{\partial^2 u}{\partial x^2}\right\rangle\right]$$
$$+\pi D\nu\left.\frac{\partial u}{\partial r}\right|_{r=D/2}+Af_x \tag{A.30}$$

Let $f_x=-\bar{\rho}gsin(\theta)$, $\tau=-\mu\left.\frac{\partial u}{\partial r}\right|_{r=D/2}$

Using Dimensionless Analysis:

Let $\hat{u}=\bar{u}/U_1$, $\hat{x}=x/L$, $\hat{P}=P/P_1=\frac{P\zeta}{\rho_o aU_1}$, $\hat{t}=t/T=\frac{ta}{\zeta L}$, $\hat{\tau}=\frac{8\tau}{\rho_o fU_1^2}$

$$\frac{aU_1}{\zeta L}\frac{\partial(\hat{u}A)}{\partial\hat{t}}+\frac{1}{2}\frac{U_1^2}{L}\frac{\partial(\beta\hat{u}^2A)}{\partial\hat{x}}=-\frac{A}{\bar{\rho}}\frac{\rho_o aU_1}{\zeta L}\frac{\partial\hat{P}}{\partial\hat{x}}-\frac{A\overline{\rho'^2}}{\bar{\rho}^3}\frac{\rho_o aU_1}{\zeta L}\frac{\partial P}{\partial x}$$
$$+(\kappa+4\mu/3)\frac{U_1}{L^2}\left[\frac{1}{\bar{\rho}}\frac{\partial^2(\hat{u}A)}{\partial\hat{x}^2}-\frac{1}{\bar{\rho}^2}A\left\langle\rho'\frac{\partial^2\hat{u}}{\partial\hat{x}^2}\right\rangle+\frac{1}{\bar{\rho}^3}A\left\langle\rho'^2\frac{\partial^2\hat{u}}{\partial\hat{x}^2}\right\rangle\right]$$
$$-\frac{\hat{\tau}\rho_o fU_1^2\pi D}{8\rho A}-A\bar{\rho}gsin(\theta) \tag{A.31}$$

multiplying the equation by $\frac{\zeta L}{aU_1}$, and assuming $M \ll 1$ where $M = \frac{U_1}{a}$ and $R_L = \frac{LU_1\rho}{\kappa+4\mu/3}$

$$\frac{\partial(\hat{u}A)}{\partial\hat{t}} + \frac{1}{2}\frac{\zeta U_1}{a}\frac{\partial(\beta\hat{u}^2A)}{\partial\hat{x}} = -\frac{A\rho_o}{\bar{\rho}}\frac{\partial\hat{P}}{\partial\hat{x}} - \frac{A\rho_o\overline{\rho'^2}}{\bar{\rho}^3}\frac{\partial P}{\partial x} + (\kappa+4\mu/3)\frac{\zeta}{aL}\left[\frac{1}{\bar{\rho}}\frac{\partial^2(\hat{u}A)}{\partial\hat{x}^2} - \frac{1}{\bar{\rho}^2}A\left\langle\rho'\frac{\partial^2\hat{u}}{\partial\hat{x}^2}\right\rangle + \frac{1}{\bar{\rho}^3}A\left\langle\rho'^2\frac{\partial^2\hat{u}}{\partial\hat{x}^2}\right\rangle\right] - \frac{\hat{\tau}\rho_o f U_1\pi DL\zeta}{2\rho\pi D^2 a} - \frac{\zeta L}{aU_1}A\bar{\rho}gsin(\theta) \tag{A.32}$$

$$\frac{\partial(\hat{u}A)}{\partial\hat{t}} + \frac{1}{2}\zeta M\frac{\partial(\beta\hat{u}^2A)}{\partial\hat{x}} = -\frac{A\rho_o}{\bar{\rho}}\frac{\partial\hat{P}}{\partial\hat{x}} - \frac{A\rho_o\overline{\rho'^2}}{\bar{\rho}^3}\frac{\partial P}{\partial x} + \frac{\zeta M}{R_L}\left[\frac{1}{\bar{\rho}}\frac{\partial^2(\hat{u}A)}{\partial\hat{x}^2} - \frac{1}{\bar{\rho}^2}A\left\langle\rho'\frac{\partial^2\hat{u}}{\partial\hat{x}^2}\right\rangle + \frac{1}{\bar{\rho}^3}A\left\langle\rho'^2\frac{\partial^2\hat{u}}{\partial\hat{x}^2}\right\rangle\right] - \frac{\hat{\tau}\rho_o fL\zeta M}{2\rho D} - \frac{\zeta L}{aU_1}A\bar{\rho}gsin(\theta) \tag{A.33}$$

$$\frac{\partial(\hat{u}A)}{\partial\hat{t}} = -\frac{A\rho_o}{\bar{\rho}}\frac{\partial\hat{P}}{\partial\hat{x}} - \frac{A\rho_o\overline{\rho'^2}}{\bar{\rho}^3}\frac{\partial P}{\partial x} - \frac{\hat{\tau}\rho_o fL\zeta M}{2\rho D} - \frac{\zeta L}{aU_1}A\bar{\rho}gsin(\theta) \tag{A.34}$$

going back to dimensional form and assuming constant Area:

$$\frac{\partial(\bar{u}A)}{\partial t} + \frac{A}{\bar{\rho}}\frac{\partial P}{\partial x} + \frac{A\overline{\rho'^2}}{\bar{\rho}^3}\frac{\partial P}{\partial x} + \frac{\pi D}{\rho}\tau + A\bar{\rho}gsin(\theta) = 0 \tag{A.35}$$

$$\frac{\partial(\bar{u})}{\partial t} + \frac{1}{\bar{\rho}}\frac{\partial P}{\partial x}\left(1 + \frac{\overline{\rho'^2}}{\bar{\rho}^2}\right) + \frac{\pi D}{\rho A}\tau + \bar{\rho}gsin(\theta) = 0 \tag{A.36}$$

Use Piezometric Head and substitute in (23):

$$P = \bar{\rho}g(\bar{h} - Z) \tag{A.37}$$

$$\frac{\partial P}{\partial x} = \bar{\rho}g\frac{\partial\bar{h}}{\partial x} - \bar{\rho}g\frac{\partial Z}{\partial x} = \bar{\rho}g\frac{\partial\bar{h}}{\partial x} - \bar{\rho}gsin(\theta) \tag{A.38}$$

$$\frac{\partial\bar{u}}{\partial t} + \frac{\bar{\rho}g}{\bar{\rho}}\frac{\partial\bar{h}}{\partial x}\left(1 + \frac{\overline{\rho'^2}}{\bar{\rho}^2}\right) + \frac{\pi D}{\rho A}\tau - \bar{\rho}gsin(\theta) + \bar{\rho}gsin(\theta) = 0 \tag{A.39}$$

let $\tau = \frac{\rho f \bar{u}|\bar{u}|}{8}$

$$\frac{\partial \bar{u}}{\partial t} + g\frac{\partial \bar{h}}{\partial x}\left(1 + \frac{\overline{\rho'^2}}{\bar{\rho}^2}\right) + \frac{\pi D}{\rho A}\tau = 0 \tag{A.40}$$

$$\frac{\partial \bar{u}}{\partial t} + g\frac{\partial \bar{h}}{\partial x}\left(1 + \frac{\overline{\rho'^2}}{\bar{\rho}^2}\right) + \frac{f\bar{u}|\bar{u}|}{2D} = 0 \tag{A.41}$$

assuming $\overline{\rho'^2} \ll 1$ leads to

$$\frac{\partial \bar{u}}{\partial t} + g\frac{\partial \bar{h}}{\partial x} + \frac{f\bar{u}|\bar{u}|}{2D} = 0 \tag{A.42}$$

A.2 Method of Characteristics

Starting with water-hammer equations

$$\frac{\partial h}{\partial t} + \frac{a^2}{g}\frac{\partial u}{\partial x} = 0 \tag{A.43}$$

$$\frac{\partial u}{\partial t} + g\frac{\partial h}{\partial x} = k|u|u, \qquad k = -\frac{f}{2D} \tag{A.44}$$

multiplying (A.43) by a multiplier, λ and adding it to (A.44) results in

$$\left[\frac{\partial u}{\partial t} + \lambda\frac{a^2}{g}\frac{\partial u}{\partial x}\right] + \lambda\left[\frac{\partial h}{\partial t} + \frac{g}{\lambda}\frac{\partial h}{\partial x}\right] = k|u|u \tag{A.45}$$

This is the total derivative for $\frac{du}{dt} = \frac{\partial u}{\partial t} + \frac{dx}{dt}\frac{\partial u}{\partial x}$ and $\frac{dh}{dt} = \frac{\partial h}{\partial t} + \frac{dx}{dt}\frac{\partial h}{\partial x}$, where $\frac{dx}{dt} = \lambda\frac{a^2}{g}$ and $\frac{dx}{dt} = \frac{g}{\lambda}$

To find λ let

$$\lambda\frac{a^2}{g} = \frac{g}{\lambda} \tag{A.46}$$

This will result in $\lambda = \pm\frac{g}{a}$. Substituting this (A.45) will result in the following equations along

the characteristic lines

$$\frac{\mathrm{d}u}{\mathrm{d}t} + \frac{g}{a}\frac{\mathrm{d}h}{\mathrm{d}t} = k|u|u, \qquad \text{along} \qquad \frac{dx}{dt} = +a \tag{A.47}$$

$$\frac{\mathrm{d}u}{\mathrm{d}t} - \frac{g}{a}\frac{\mathrm{d}h}{\mathrm{d}t} = k|u|u, \qquad \text{along} \qquad \frac{dx}{dt} = -a \tag{A.48}$$

B Method of Distributions

B.1 Derivation of PDF Equations

The derivation of a PDF equation starts by defining a "raw" PDF function (Tartakovsky & Gremaud 2015),

$$\Pi(U-u,H-h) = \delta[U-u(x,t)]\delta[H-h(x,t)], \tag{B.1}$$

where $\delta(\cdot)$ is the Dirac delta function. Its ensemble mean, over the realization of random variables u and h at the space-time point (x,t), is the joint PDF $f_{uh}(U,H;x,t)$:

$$\mathbb{E}[\Pi] \equiv \int_{-\infty}^{\infty}\int_{-\infty}^{\infty} \delta(U-\mathcal{U})\delta(H-\mathcal{H}) f_{uh}(\mathcal{U},\mathcal{H};x,t)\mathrm{d}\mathcal{H}\mathrm{d}\mathcal{U} = f_{uh}(U,H;x,t). \tag{B.2}$$

Recalling the sifting property of the Dirac delta function, $r(u)\delta(U-u) = r(U)\delta(U-u)$; noting that

$$\frac{\partial \Pi}{\partial t} = \frac{\partial \Pi}{\partial h}\frac{\partial h}{\partial t} + \frac{\partial \Pi}{\partial u}\frac{\partial u}{\partial t} = -\frac{\partial \Pi}{\partial H}\frac{\partial h}{\partial t} - \frac{\partial \Pi}{\partial U}\frac{\partial u}{\partial t}; \tag{B.3}$$

multiplying (2.1a) by $-\partial\Pi/\partial H$ and (2.1b) by $-\partial\Pi/\partial U$; and adding the resulting equations together leads to

$$\frac{\partial \Pi}{\partial t} - \frac{\partial \Pi}{\partial H}\frac{a^2}{g}\frac{\partial u}{\partial x} - \frac{\partial \Pi}{\partial U} g\frac{\partial h}{\partial x} = -\frac{\partial}{\partial U}[r(U)\Pi] - \frac{1}{A}\delta(x-x_{\text{leak}})\frac{\partial Q_{\text{leak}}(H)\Pi}{\partial H}. \tag{B.4}$$

Because of Reynolds' decompositions of the variables involved, including $\Pi = f_{uh} + \Pi'$, the ensemble mean of this equation is

$$\frac{\partial f_{uh}}{\partial t} + \frac{\partial}{\partial H}\left[Q_1 - \frac{a^2}{g}\frac{\partial \bar{u}}{\partial x} f_{uh} + \frac{Q_{\text{leak}}(H)}{A}\delta(x-x_{\text{leak}}) f_{uh}\right] + \frac{\partial}{\partial U}\left[Q_2 - g\frac{\partial \bar{h}}{\partial x} f_{uh} + k|U|U f_{uh}\right] = 0 \tag{B.5}$$

where

$$Q_1 = -\frac{a^2}{g}\mathbb{E}\left[\frac{\partial u'}{\partial x}\Pi'\right] \qquad \text{and} \qquad Q_2 = -g\mathbb{E}\left[\frac{\partial h'}{\partial x}\Pi'\right]. \tag{B.6}$$

As a closure approximation, we postulate that

$$Q_1 = \alpha_1(x,t)[H-\bar{h}(x,t)]f_{uh} \qquad \text{and} \qquad Q_2 = \alpha_2(x,t)[U-\bar{u}(x,t)]f_{uh}. \tag{B.7}$$

The coefficients $\alpha_1(x,t)$ and $\alpha_2(x,t)$ are obtained by ensuring that the PDF f_{uh} in (B.5) has the same means, $\bar{u}$ and $\bar{h}$, and variances, σ_u^2 and σ_h^2, as those resulted from the moment differential equations (B.18), (B.19), (B.22) and (B.23). To derive an expression for $\alpha_1(x,t)$, we recall that $f_h(H;x,t) = \int f_{uh}\mathrm{d}U$ so that the integration of (B.5) with (B.7) over U yields an equation for $f_h(H;x,t)$,

$$\frac{\partial f_h}{\partial t} + \frac{\partial}{\partial H}\left[\alpha_1(H-\bar{h})f_h - \frac{a^2}{g}\frac{\partial \bar{u}}{\partial x}f_h + \frac{Q_{\text{leak}}(H)}{A}\delta(x-x_{\text{leak}})f_h\right] = 0, \tag{B.8}$$

which relies on the boundary condition $f_{uh}(\pm\infty,H;x,t) = 0$. We rely on a truncated Taylor expansion around the mean value to approximate

$$\mathbb{E}[\sqrt{h}] \approx \sqrt{\bar{h}} - \frac{\sigma_h^2}{8\bar{h}\sqrt{\bar{h}}} \qquad \text{and} \qquad \mathbb{E}[\sqrt{h}h] \approx \bar{h}\sqrt{\bar{h}} + \frac{3\sigma_h^2}{8\sqrt{\bar{h}}}.$$

Moreover, since $\int_{-\infty}^{\infty} f_h \mathrm{d}H = 1$ and $\int_{-\infty}^{\infty} H f_h \mathrm{d}H = \bar{h}$, and since $f_h(\pm\infty;x,t) = 0$ such that the limit $\lim_{H\to\pm\infty}[H f_h(H;x,t)] = 0$, multiplying the above equation by H and integrating it over H leads to (B.18). This means that the closure for Q_1 preserves the mean, regardless of the choice of $\alpha_1(x,t)$. To compute the variance of f_h, i.e., $\sigma_h^2 = \int_{-\infty}^{\infty}(H-\bar{h})^2 f_h \mathrm{d}H$, we multiply (B.8) by $(H-\bar{h})^2$ and integrate over H. This gives an equation for the variance,

$$\frac{\partial \sigma_h^2}{\partial t} - 2\alpha_1\sigma_h^2 = \frac{\gamma_{\text{leak}}\sigma_h^2}{A\sqrt{\bar{h}}}\delta(x-x_{\text{leak}}). \tag{B.9}$$

For this equation to be consistent with (B.22), the coefficient α_1 in the closure approximation (B.7)

has to be

$$\alpha_1 = -\frac{1}{2\sigma_h^2}\beta_1. \tag{B.10}$$

Combining this with the expression for β_1 derived in Appendix B.2 leads to (2.3c).

Determination of $\alpha_2(x,t)$ follows a similar procedure. An equation for the marginal PDF $f_u(U;x,t) = \int f_{uh}\mathrm{d}H$ is derived by integrating (B.5) with (B.7) over H, while accounting for the boundary conditions $f_{uh}(U,\pm\infty;x,t) = 0$,

$$\frac{\partial f_u}{\partial t} + \frac{\partial}{\partial U}\left[\alpha_2(x,t)(U-\bar{u})f_u - g\frac{\partial \bar{h}}{\partial x}f_u + k|U|Uf_u\right] = 0. \tag{B.11}$$

Multiplying this equation with U, integrating the result over U, and accounting for the boundary condition $f_u(\pm\infty;x,t) = 0$, yields

$$\frac{\partial \bar{u}}{\partial t} + g\frac{\partial \bar{h}}{\partial x} - \int_{-\infty}^{\infty} k|U|Uf_u\mathrm{d}U = 0. \tag{B.12}$$

Expanding $\mathbb{E}[|u|u]$ into the truncated Taylor series (B.16), we obtain $\mathbb{E}[|u|u] \approx |\bar{u}|\bar{u} + \mathrm{sgn}(\bar{u})\sigma_u^2$, so that (B.12) reduces to (B.19) for any choice of $\alpha_2(x,t)$. Multiplying (B.11) by $(U-\bar{u})^2$ and integrating over U results in

$$\frac{\partial \sigma_u^2}{\partial t} - 2\alpha_2\sigma_u^2 = 2k\mathbb{E}[|u|u^2] - 2k\bar{u}\mathbb{E}[|u|u]. \tag{B.13}$$

The second-order Taylor expansions $\mathbb{E}[|u|u] \approx |\bar{u}|\bar{u} + (|\bar{u}|/\bar{u})\sigma_u^2$ and $\mathbb{E}[|u|u^2] \approx |\bar{u}|\bar{u}^2 + 3k|\bar{u}|\sigma_u^2$ reduce (B.13) to

$$\frac{\partial \sigma_u^2}{\partial t} - 2\alpha_2\sigma_u^2 = 4k|\bar{u}|\sigma_u^2. \tag{B.14}$$

This the variance equation is consistent with (B.23) if

$$\alpha_2 = -\frac{1}{2\sigma_u^2}\beta_2. \tag{B.15}$$

Combining this with the expression for β_2 derived in Appendix B.2 leads to (2.3c).

B.2 Derivation of Moments Equations

We use the Reynolds decomposition to represent random quantities (e.g., u) as the sums of their ensemble means (e.g., $\bar{u}$) and zero-mean random fluctuations (e.g., u'). Next, we decompose the nonlinear terms $Q_{\text{leak}} = \gamma_{\text{leak}}\sqrt{h}$ and $r(u) = k|u|u$ in (2.1b) into a Taylor series about $\bar{h}$ and $\bar{u}$, respectively, such that

$$\begin{aligned} Q_{\text{leak}}(h) &= Q_{\text{leak}}(\bar{h}) + \frac{\mathrm{d}Q_{\text{leak}}}{\mathrm{d}h}(\bar{h})h' + \frac{1}{2}\frac{\mathrm{d}^2 Q_{\text{leak}}}{\mathrm{d}h^2}(\bar{h})(h')^2 + O(h'^3) \\ &= \gamma_{\text{leak}}\sqrt{\bar{h}} + \frac{\gamma_{\text{leak}}}{2\sqrt{\bar{h}}}h' - \frac{\gamma_{\text{leak}}}{8\bar{h}\sqrt{\bar{h}}}(h')^2 + O(h'^3) \end{aligned} \tag{B.16}$$

$$r(u) = r(\bar{u}) + \frac{\mathrm{d}r}{\mathrm{d}u}(\bar{u})u' + \frac{1}{2}\frac{\mathrm{d}^2 r}{\mathrm{d}u^2}(\bar{u})(u')^2 + O(u'^3) = k|\bar{u}|\bar{u} + 2k\frac{\bar{u}^2}{|\bar{u}|}u' + k\frac{\bar{u}}{|\bar{u}|}(u')^2 + O(u'^3). \tag{B.17}$$

Taking the ensemble mean of the resulting version of (2.1) yields

$$\frac{\partial \bar{h}}{\partial t} + \frac{a^2}{g}\frac{\partial \bar{u}}{\partial x} = \left(\frac{\gamma_{\text{leak}}\sqrt{\bar{h}}}{A} - \frac{\sigma_{\bar{h}}^2\gamma_{\text{leak}}}{8A\bar{h}\sqrt{\bar{h}}}\right)\delta(x - x_{\text{leak}}) \tag{B.18}$$

$$\frac{\partial \bar{u}}{\partial t} + g\frac{\partial \bar{h}}{\partial x} = k|\bar{u}|\bar{u} + k\frac{\bar{u}}{|\bar{u}|}\sigma_u^2. \tag{B.19}$$

Subtracting these from the expanded version of (2.1) leads an equation for perturbations,

$$\frac{\partial h'}{\partial t} + \frac{a^2}{g}\frac{\partial u'}{\partial x} = \left(\frac{\gamma_{\text{leak}}h'}{2A\sqrt{\bar{h}}} - \frac{\gamma_{\text{leak}}(h')^2}{8A\bar{h}\sqrt{\bar{h}}} + \frac{\gamma_{\text{leak}}\sigma_{\bar{h}}^2}{8A\bar{h}\sqrt{\bar{h}}}\right)\delta(x - x_{\text{leak}}) \tag{B.20}$$

$$\frac{\partial u'}{\partial t} + g\frac{\partial h'}{\partial x} = 2k|\bar{u}|u' + k\frac{\bar{u}}{|u|}(u')^2 - k\frac{\bar{u}}{|\bar{u}|}\sigma_u^2. \tag{B.21}$$

Multiplying (B.20) by $h'(x,t)$ and (B.21) by $u'(x,t)$, and taking the ensemble average of the resulting equations leads to

$$\frac{\partial \sigma_h^2}{\partial t} + \beta_1 = \frac{\gamma_{\text{leak}} \sigma_h^2}{A\sqrt{\bar{h}}} \delta(x - x_{\text{leak}}), \qquad \beta_1 = \frac{2a^2}{g} \mathbb{E}\left[h' \frac{\partial u'}{\partial x} \right] \tag{B.22}$$

$$\frac{\partial \sigma_u^2}{\partial t} + \beta_2 = 4k|\bar{u}|\sigma_u^2, \qquad \beta_2 = 2g\mathbb{E}\left[u' \frac{\partial h'}{\partial x} \right]. \tag{B.23}$$

B.3 Initial Conditions for PDF Equation

The lognormal PDF $f_{u_0}(U)$ of the initial velocity $u_0 = 2.0 + 0.1\exp(z)$ with Gaussian z is given by

$$f_{u_0}(U) = \left| \frac{\mathrm{d}z}{\mathrm{d}u_0} \right| f_z = \frac{1}{\sqrt{2\pi}(U-2)\sigma_z} \exp\left[-\frac{[\ln(10(U-2)) - \mu_z]^2}{2\sigma_z^2} \right], \qquad U > 2. \tag{B.24}$$

This distribution is used as the initial condition for the PDF equation before the first contact discontinuity reaches the point of interest $x^\star$, i.e., during the time interval $0 \le t < \tau^\star$. Given the deterministic relation between h_0 and u_0 in (2.2b), the conditional PDF $f_{h_0|u_0}$ is

$$f_{h_0|u_0}(H;U;x) = \delta(H - H_{\text{in}} - \frac{kx}{g}|U|U). \tag{B.25}$$

The initial condition for the joint PDF equation (2.3), defined on the time interval $0 \le t < \tau^\star$, is $f_{u_0 h_0}(U,H;x) = f_{h_0|u_0} f_{u_0}$.

An equation for characteristics of the WHE (2.1),

$$\frac{\mathrm{d}x}{\mathrm{d}t} = \pm a, \tag{B.26}$$

defines two families of characteristics, $x(t) = at + \xi_+$ and $x(t) = -at + \xi_-$, where the constants of integration $\xi_\pm = x(0)$ label individual characteristics within each family. Specifically, the

characteristic that carries backward the first contact discontinuity originating at the moment of the valve closure, $x(0) = L$, is labeled with $\xi_- = L$ (Fig. 2.1). The wave traveling along this characteristic, $x(t) = -at + L$, reaches the observation point $x^\star = L/2$ at time $t \equiv \tau^\star = L/(2a)$. A characteristic from the family of characteristics $x(t) = at + \xi_+$, which intersects the characteristic $x(t) = -at + L$ at the space-point point $(x^\star, \tau^\star)$ is labeled by $\xi_+ = 0$, i.e., has the equation $x(t) = at$ (Fig. 2.1).

Along all characteristics defined by (B.26), including those specified by equations $x(t) = at$ and $x(t) = -at + L$, the state variables $u(x(t),t)$ and $h(x(t),t)$ satisfy

$$\frac{\mathrm{d}u(x(t),t)}{\mathrm{d}t} = \frac{\partial u}{\partial t} \pm a\frac{\partial u}{\partial x} \qquad \text{and} \qquad \frac{\mathrm{d}h(x(t),t)}{\mathrm{d}t} = \frac{\partial h}{\partial t} \pm a\frac{\partial h}{\partial x}. \tag{B.27}$$

Hence, the WHE (2.1) transform into

$$\frac{\mathrm{d}u}{\mathrm{d}t} \pm \frac{g}{a}\frac{\mathrm{d}h}{\mathrm{d}t} = k|u|u \pm \frac{g}{a}\frac{Q_{\text{leak}}}{A}\delta(x - x_{\text{leak}}), \tag{B.28}$$

such that the equations with the plus and minus signs are defined along the characteristics $x(t) = at$ and $x(t) = -at + L$, respectively.

B.3.1 PDFs of u and h at the first contact discontinuity

Integrating (B.28) for the characteristic $x(t) = at$ from 0 to $\tau^\star$, while accounting for the initial conditions $u[x(0) = 0, t = 0] = u_0$ and $h[x(0) = 0, t = 0] = H_{\text{in}}$, yields

$$u_1 - u_0 + \frac{g}{a}(h_1 - H_{\text{in}}) = k\int_0^{\tau^\star} |u|\,u\,\mathrm{d}t + \frac{g}{aA}\int_0^{\tau^\star} Q_{\text{leak}}\delta(at - x_{\text{leak}})\mathrm{d}t, \tag{B.29}$$

where $u_1 = u(x^\star, \tau^\star)$ and $h_1 = h(x^\star, \tau^\star)$. In the absence of a leak ($Q_{\text{leak}} = 0$), the one-dimensional velocity u along the characteristic $x = at$ remains constant, $u = u_0 > 0$, for $t < \tau^\star$. Hence, (B.29)

reduces to

$$u_1 - u_0 + \frac{g}{a}(h_1 - H_{\text{in}}) = k\tau^\star u_0^2. \tag{B.30}$$

Integrating (B.28) on the characteristic $x(t) = -at + L$ from 0 to $\tau^\star$, while accounting for the initial conditions $u[x(0) = L, t = 0] = 0$ and $h[x(0) = L, t = 0] = H_{\text{in}} + (kL/g)u_0^2 + (a/g)u_0$ obtained from (2.2b), yields

$$u_1 + u_0 - \frac{g}{a}(h_1 - H_{\text{in}} - \frac{kL}{g}u_0^2) = k\int_0^{\tau^\star} |u|\, u \, \mathrm{d}t - \frac{g}{aA}\int_0^{\tau^\star} Q_{\text{leak}}\delta(-at + L - x_{\text{leak}})\mathrm{d}t. \tag{B.31}$$

For $Q_{\text{leak}} = 0$, the first integral on the right-hand side is approximately 0 since $u(L, 0) = 0$, which yields

$$u_1 + u_0 - \frac{g}{a}(h_1 - H_{\text{in}} - \frac{kL}{g}u_0^2) = 0. \tag{B.32}$$

(The impact of this approximation on the accuracy of our PDF method is investigated via comparison with MCS.) Recalling that $L/a = 2\tau^\star$, it follows from (B.30) and (B.32) that

$$u_1 = -\frac{k\tau^\star}{2}|u_0^2 \qquad \text{or} \qquad u_0 = \sqrt{-\frac{2}{k\tau^\star}u_1}. \tag{B.33}$$

Substituting this expression into (B.30) gives the corresponding value of h_1,

$$h_1 = H_{\text{in}} + \frac{a}{g}\left(u_0 + \frac{3k\tau^\star}{2}u_0^2\right). \tag{B.34}$$

Since the function $U_0 = U_0(U_1)$ in (B.33) is monotonic, the PDF of u_1, $f_{u_1}(U)$, is obtained as $f_{u_1}(U) = |\mathrm{d}U_0/\mathrm{d}U_1(U)| f_{u_0}(U_0(U))$ resulting in

$$f_{u_1}(U) = \frac{1}{\sqrt{-2k\tau^\star U}} f_{u_0}(U_0(U)), \qquad U > 0. \tag{B.35}$$

Given the deterministic relations between h_1 and u_1 in (B.34) and between u_0 and u_1 in (B.33), the conditional PDF $f_{h_1|u_1}(H;U)$ is the Dirac delta function,

$$f_{h_1|u_1} = \delta\left(H - H_{\mathrm{in}} - \frac{a}{g}\sqrt{-\frac{2U}{k\tau^\star}} + \frac{3a}{g}U\right). \tag{B.36}$$

Finally, the joint PDF for u_1 and h_1 is obtained as $f_{u_1 h_1} = f_{h_1|u_1} f_{u_1}$.

B.3.2 PDFs of u and h at the second contact discontinuity

The second contact discontinuity originates at (and is reflected from) the inlet boundary $x(t) = 0$ at time $t = \tau$; it travels along the characteristic line $x(t) = at + \xi_+$ with $\xi_+ = -L$, and reaches the point $x^\star = L/2$ at time $t = 2\tau - \tau^\star$ (Fig. 2.1). At the space-time point $(x^\star = L/2, t = 2\tau - \tau^\star)$, this characteristic line intersects with the characteristic line $x(t) = -at + \xi_-$ labeled by $\xi_- = 2L$.

The two PDEs in (B.28), to be solved along the characteristics $x(t) = at - L$ and $x(t) = -at + 2L$, need boundary conditions at the space-time points $\{x(\tau) = 0, \tau\}$ and $\{x(\tau) = L, \tau\}$, respectively. The value of $h[x(t), t]$ at the point $\{0, \tau\}$ is $h[x(\tau) = 0, \tau] = H_{\mathrm{in}}$, while the corresponding boundary value for $u[x(t), t]$ is obtained by integrating in time, from 0 to τ, the PDE (B.28) along the characteristic $x(t) = -at + L$. This equation is subject to the auxiliary conditions

$$u[x(0) = L, 0] = 0, \qquad h[x(0) = L, 0] = H_{\mathrm{in}} + \frac{kL}{g}u_0^2 + \frac{a}{g}u_0.$$

Since in the absence of the leak ($Q_{\mathrm{leak}} = 0$), $u \approx 0$ for $t < \tau$ along the characteristics $x(t) = -at + L$,

and accounting for these boundary conditions, the time integration of the respective PDE (B.28) yields the required value of $u[x(t),t]$ at the point $\{0,\tau\}$,

$$u[x(\tau)=0,\tau] = -u_0 - \frac{kL}{a}u_0^2. \tag{B.37}$$

Likewise, the value of $u[x(t),t]$ at the point $\{x(\tau)=L,\tau\}$ is $u[x(\tau)=L,\tau]=0$. The corresponding boundary value for $h[x(t),t]$ is obtained by integrating in time, from 0 to τ, the PDE (B.28) along the characteristic $x(t)=at$. This equation is subject to the auxiliary conditions

$$u[x(0)=0,0]=u_0, \qquad h[x(0)=0,0]=H_{\text{in}}.$$

A solution of this boundary-value problem is

$$-u_0 + \frac{g}{a}(h[x(\tau)=L,\tau]-H_{\text{in}}) = k\int_0^\tau |u|u\mathrm{d}\tau'. \tag{B.38}$$

According to the fundamental theorem of integral calculus, $\int_0^\tau g(\tau')\mathrm{d}\tau' = g(\xi)\tau$ with $0<\xi<\tau$; as an approximation, we choose $g(\xi)=[g(0)+g(\tau)]/2$. Since $u(L,\tau)=0$, this leads to the required value of $h[x(t),t]$ at the point $\{L,\tau\}$,

$$h[x(\tau)=L,\tau] = H_{\text{in}} + \frac{a}{g}\left(u_0 + \frac{k\tau}{2}u_0^2\right). \tag{B.39}$$

With these boundary conditions, and in the absence of leaks, the initial-value problem (B.28) along the characteristic $x=at-L$ is

$$\frac{\mathrm{d}u}{\mathrm{d}t} + \frac{g}{a}\frac{\mathrm{d}h}{\mathrm{d}t} = k|u|u, \qquad h[x(\tau)=0,\tau]=H_{\text{in}}, \qquad u[x(\tau)=0,\tau]=-u_0-k\tau u_0^2.$$

Integrating this problem from τ to $2\tau-\tau^\star$ yields the values of u and h at the second contact

discontinuity (Fig. 2.1), $u_2 \equiv u(x^\star, 2\tau - \tau^\star)$ and $h_2 \equiv h(x^\star, 2\tau - \tau^\star)$,

$$u_2 + u_0 + k\tau u_0^2 + \frac{g}{a}(h_2 - H_{\text{in}}) = -k(\tau - \tau^\star)(u_0 + k\tau u_0^2)^2. \tag{B.40}$$

This equation is derived by assuming that $u \approx u[x(\tau) = 0, \tau] = -u_0 - k\tau u_0^2$ for $\tau < t < 2\tau - \tau^\star$. Likewise the initial-value problem (B.28) along the characteristic $x = -at + 2L$ is

$$\frac{\mathrm{d}u}{\mathrm{d}t} - \frac{g}{a}\frac{\mathrm{d}h}{\mathrm{d}t} = k|u|u, \qquad h[x(\tau) = L, \tau] = H_{\text{in}} + \frac{a}{g}\left(u_0 + \frac{k\tau}{2}u_0^2\right), \qquad u[x(\tau) = L, \tau] = 0.$$

Integrating this problem from τ to $2\tau - \tau^\star$, while accounting for the fact that $u \approx 0$ for $\tau < t < 2\tau - \tau^\star$, yields

$$u_2 - \frac{g}{a}(h_2 - H_{\text{in}}) - \left(u_0 - \frac{k\tau}{2}u_0^2\right) = 0. \tag{B.41}$$

A solution of (B.40) and (B.41) for u_2 is a fourth-degree polynomial in u_0,

$$u_2 = -\frac{k^3(\tau - \tau^\star)\tau^2}{2}u_0^4 - k^2(\tau - \tau^\star)\tau u_0^3 - k\tau u_0^2 - u_0. \tag{B.42}$$

This polynomial has four roots. We approximate the root, u_0, on the interval of interest, $u_0 = 2.0 + 0.1\exp(z)$ with $z \sim \mathcal{N}(0, 0.4^2)$, as

$$u_0 = \alpha u_2^2 + \beta u_2 + \gamma. \tag{B.43}$$

The constants α, β, and γ are obtained by fitting (via minimization of the mean root square errors) the parabola in (B.43) to the array of $\{u_{0_i}, u_{2_i}\}_{i=1}^N$ obtained from (B.42). (The second-degree polynomial (B.43) turned out to provide a better fit than the first-degree polynomial.) Figure B.1 shows the agreement between the graphs of $u_0 = u_0(u_2)$ obtained, alternatively, from (B.42) and (B.43) on the domain of interest. The figure also demonstrates the agreement between these relations and the solution $u_2 = u_2(u_0)$ computed with multiple solves of the original WHE (2.1)

for different values of u_0. It serves to validate the approximations we have made to derive the analytical expressions for u_i and h_i with $i = 1, 2$.

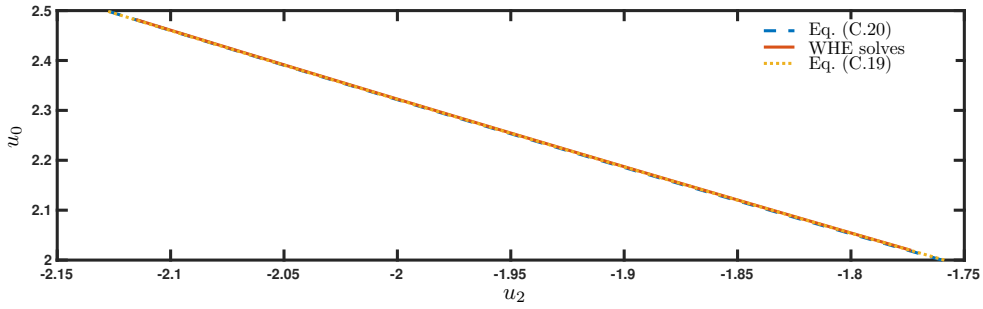

Figure B.1: The relationship between u_0 and u_2 computed, alternatively, with (B.42), (B.43), and multiple solves of the WHE (2.1) for different values of u_0. This relationship is monotonic in the region of interest.

Substituting (B.43) into (B.41) gives an expression for h_2

$$h_2 = H_{\text{in}} + \frac{a}{g}u_2 + \frac{a}{g}(\alpha u_2^2 + \beta u_2 + \gamma) + \frac{ka\tau^\star}{g}\left|\alpha u_2^2 + \beta u_2 + \gamma\right|(\alpha u_2^2 + \beta u_2 + \gamma). \tag{B.44}$$

Since the function $u_0 = u_0(u_2)$ is monotonic in the region of interest (Fig. B.1), the corresponding PDFs are

$$f_{u_2} = \left|\frac{\mathrm{d}u_0}{\mathrm{d}u_2}\right| f_{u_0} = \frac{|2\alpha U + \beta|}{(\alpha U^2 + \beta U + \gamma - 2)\sigma\sqrt{2\pi}} \exp\left(\frac{-[\ln(10(\alpha U^2 + \beta U + \gamma - 2)) - \mu]^2}{2\sigma^2}\right) \tag{B.45}$$

$$f_{h_2|u_2} = \delta\left(H - H_{\text{in}} - \frac{a}{g}U - \frac{a}{g}(\alpha U^2 + \beta U + \gamma) - \frac{ka\tau^\star}{g}\left|\alpha U^2 + \beta U + \gamma\right|(\alpha U^2 + \beta U + \gamma)\right) \tag{B.46}$$

$$f_{u_2 h_2} = f_{h_2|u_2} f_{u_2}. \tag{B.47}$$

The same procedure can be repeated after each contact discontinuity, until $t = t_{\max}$.

Bibliography

Alawadhi, A., Boso, F. & Tartakovsky, D. M. (2018), 'Method of distributions for water-hammer equations with uncertain parameters', *Water Resour. Res.* **54**(11), 9398–9411.

Alawadhi, A. & Tartakovsky, D. M. (2019), 'Bayesian updating and method of distributions: Application to leak detection in pipes', *To be pubished* .

ASCE (2015), 2013 report card for America's infrastructures, Technical report, American Society of Civil Engineers. www.infrastructurereportcard.org/a/documents/2013-Report-Card.pdf.

Bannister, R. N. (2017), 'A review of operational methods of variational and ensemble-variational data assimilation', *Quart. J. Roy. Meteor. Soc.* **143**(703), 607–633.

Barajas-Solano, D. A. & Tartakovsky, D. M. (2016), 'Stochastic collocation methods for nonlinear parabolic equations with random coefficients', *SIAM/ASA J. Uncert. Quant.* **4**(1), 475–494.

Brothers, K. J. (2001), 'Water leakage and sustainable supply – truth or consequences?', *J. Am. Water Works Assoc.* **93**(4), 150–152.

Brunone, B. (1999), 'Transient test-based technique for leak detection in outfall pipes', *J. Water Resour. Plan. Manage.* **125**(5), 302–306.

Brunone, B. & Ferrante, M. (2001), 'Detecting leaks in pressurised pipes by means of transients', *J. Hydraul. Res.* **39**(5), 539–547.

Brunone, B., Ferrante, M. & Meniconi, S. (2008), 'Portable pressure wave-maker for leak detection and pipe system characterization', *J. Am. Water Works Assoc.* **100**(4), 108–116.

Chaudhry, M. H. (2013), *Applied Hydraulic Transients*, 3 edn, Springer.

Colombo, A. F., Lee, P. & Karney, B. W. (2009), 'A selective literature review of transient-based leak detection methods', *J. Hydro Environ. Res.* **2**(4), 212–227.

Covas, D. & Ramos, H. (2010), 'Case studies of leak detection and location in water pipe systems by inverse transient analysis', *Journal of Water Resources Planning and Management* **136**(2), 248–257.

Covas, D., Ramos, H. & De Almeida, A. B. (2005), 'Standing wave difference method for leak detection in pipeline systems', *J. Hydraul. Eng.* **131**(12), 1106–1116.

Covas, D., Ramos, H., Lopes, N. & Almeida, A. B. (2008), Water pipe system diagnosis by transient pressure signals, *in* 'Water Distribution Systems Analysis Symposium 2006', pp. 1–19.

Demirci, S., Yigit, E., Eskidemir, I. H. & Ozdemir, C. (2012), 'Ground penetrating radar imaging of water leaks from buried pipes based on back-projection method', *Ndt & E International* **47**, 35–42.

Duan, H.-F. (2015), 'Uncertainty analysis of transient flow modeling and transient-based leak detection in elastic water pipeline systems', *Water Resour. Manag.* **29**(14), 5413–5427.

Fletcher, R. & Chandrasekaran, M. (2008), Smartball^{TM}: a new approach in pipeline leak detection, *in* '2008 7th International Pipeline Conference', American Society of Mechanical Engineers, pp. 117–133.

Gao, Y., Brennan, M. & Joseph, P. (2009), 'On the effects of reflections on time delay estimation for leak detection in buried plastic water pipes', *Journal of Sound and Vibration* **325**(3), 649–663.

Ghazali, M., Beck, S., Shucksmith, J., Boxall, J. & Staszewski, W. (2012), 'Comparative study of instantaneous frequency based methods for leak detection in pipeline networks', *Mechanical Systems and Signal Processing* **29**, 187–200.

Guo, X., Zhang, L., Liang, W. & Haugen, S. (2018), 'Risk identification of third-party damage on oil and gas pipelines through the Bayesian network', *J. Loss Prevent. Proc.* **54**, 163–178.

Hargesheimer, E. E. (1985), 'Identifying water main leaks with trihalomethane tracers', *Journal-American Water Works Association* **77**(11), 71–75.

Jönsson, L. & Larson, M. (1992), Leak detection through hydraulic transient analysis, *in* 'Pipeline systems', Springer, pp. 273–286.

Kapelan, Z. S., Savic, D. A. & Walters, G. A. (2003), 'A hybrid inverse transient model for leakage detection and roughness calibration in pipe networks', *Journal of Hydraulic Research* **41**(5), 481–492.

Karim, M. R., Abbaszadegan, M. & LeChevallier, M. (2003), 'Potential for pathogen intrusion during pressure transients', *Journal-American Water Works Association* **95**(5), 134–146.

Kirmeyer, G. J. & Martel, K. (2001), *Pathogen intrusion into the distribution system*, American Water Works Association.

Lee, P. J., Duan, H.-F., Vítkovskỳ, J. P., Zecchin, A. & Ghidaoui, M. (2013), 'The effect of time–frequency discretization on the accuracy of the transmission line modelling of fluid transients', *Journal of Hydraulic Research* **51**(3), 273–283.

Lee, P. J., Vítkovskỳ, J. P., Lambert, M. F., Simpson, A. R. & Liggett, J. A. (2005), 'Frequency domain analysis for detecting pipeline leaks', *J. Hydraul. Eng.* **131**(7), 596–604.

Liggett, J. A. & Chen, L.-C. (1994), 'Inverse transient analysis in pipe networks', *J. Hydraul. Eng.* **120**(8), 934–955.

Massari, C., Yeh, T.-C. J., Brunone, B., Ferrante, M. & Meniconi, S. (2013), 'Diagnosis of pipe systems by means of a stochastic successive linear estimator', *Water Resour. Manage.* **27**(13), 4637–4654.

Massari, C., Yeh, T.-C. J., Ferrante, M., Brunone, B. & Meniconi, S. (2013), 'Diagnosis of pipe systems by the SLE: first results', *Water Sci. Technol.* **13**(4), 958–965.

Massari, C., Yeh, T.-C. J., Ferrante, M., Brunone, B. & Meniconi, S. (2014), 'Detection and sizing of extended partial blockages in pipelines by means of a stochastic successive linear estimator', *J. Hydroinform.* **16**(2), 248–258.

Meniconi, S., Brunone, B., Ferrante, M., Capponi, C., Carrettini, C. A., Chiesa, C., Segalini, D. & Lanfranchi, E. A. (2015), 'Anomaly pre-localization in distribution–transmission mains by pump trip: preliminary field tests in the Milan pipe system', *J. Hydroinform.* **17**(3), 377–389.

Mergelas, B. & Henrich, G. (2005), 'Leak locating method for precommissioned transmission pipelines: North american case studies', *Leakage 2005* pp. 12–14.

Mpesha, W., Gassman, S. L. & Chaudhry, M. H. (2001), 'Leak detection in pipes by frequency response method', *J. Hydraul. Eng.* **127**(2), 134–147.

Muggleton, J. & Brennan, M. (2004), 'Leak noise propagation and attenuation in submerged plastic water pipes', *Journal of Sound and Vibration* **278**(3), 527–537.

Neuman, S., Tartakovsky, D., Wallstrom, T. & Winter, C. (1996), 'Correction to prediction of steady state flow in nonuniform geologic media by conditional moments: Exact nonlocal formalism, effective conductivities, and weak approximation', *Water Resour. Res* **32**(5), 1479–1480.

O'Brien, E., Murray, T. & McDonald, A. (2003), 'Detecting leaks from water pipes at a test facility using ground-penetrating radar', *Proceedings of Pumps, Electromechanical Devices and Systems Applied to Urban Water Management* .

Ratcliffe, B. & Field, D. (1978), *Location of leaks in pressurised pipelines using sulphur hexafluoride as a tracer*, Water Research Centre.

Rougier, J. & Goldstein, M. (2001), 'A Bayesian analysis of fluid flow in pipe-lines', *J. Roy. Stat. Soc. C* **50**(1), 77–93.

Sattar, A. M. A. & El-Beltagy, M. (2016), 'Stochastic solution to the water hammer equations using polynomial chaos expansion with random boundary and initial conditions', *J. Hydraul. Eng.* **143**(2), 04016078.

Soares, A. K., Covas, D. I. & Reis, L. F. R. (2011), 'Leak detection by inverse transient analysis in an experimental pvc pipe system', *Journal of Hydroinformatics* **13**(2), 153–166.

Taghvaei, M., Beck, S. B. M. & Boxall, J. B. (2010), 'Leak detection in pipes using induced water hammer pulses and cepstrum analysis', *Int. J. COMADEM* **13**(1), 19.

Tartakovsky, D. M. & Gremaud, P. A. (2015), Method of distributions for uncertainty quantification, *in* R. Ghanem, et al., ed., 'Handbook of Uncertainty Quantification', Springer, pp. 1–22.

Thornton, J., Sturm, R. & Kunkel, G. (2008), *Water Loss Control*, 2 edn, McGraw Hill, New York.

Vítkovskỳ, J. P., Lambert, M. F., Simpson, A. R. & Liggett, J. A. (2007), 'Experimental observation and analysis of inverse transients for pipeline leak detection', *J. Water Resour. Plan. Manage.* **133**(6), 519–530.

Vítkovskỳ, J. P., Simpson, A. R. & Lambert, M. F. (2000), 'Leak detection and calibration using transients and genetic algorithms', *J. Water Resour. Plan. Manage.* **126**(4), 262–265.

Wang, X.-J., Lambert, M. F., Simpson, A. R., Liggett, J. A. & Vítkovskỳ, J. P. (2002), 'Leak detection in pipelines using the damping of fluid transients', *J. Hydraul. Eng.* **128**(7), 697–711.

Wikle, C. K. & Berliner, L. M. (2007), 'A Bayesian tutorial for data assimilation', *Physica D* **230**(1-2), 1–16.

Wylie, E. B., Streeter, V. L. & Suo, L. (1993), *Fluid Transients in Systems*, Vol. 1, 2 edn, Prentice Hall, Englewood Cliffs, NJ.

Ye, G. & Fenner, R. (2010), 'Kalman filtering of hydraulic measurements for burst detection in water distribution systems', *J. Pipeline Syst. Eng.* **2**(1), 14–22.

Zhang, Q., Karney, B., Suo, L. & Colombo, A. F. (2011), 'Stochastic analysis of water hammer and applications in reliability-based structural design for hydro turbine penstocks', *J. Hydraul. Eng.* **137**(11), 1509–1521.